THE GEOLOGICAL SOCIETY OF AMERICA®

Architecture and permeability structure of the Sibillini Mts. Thrust and influence upon recent, extension-related seismicity in the central Apennines (Italy) through fault-valve behavior

Manuel Curzi[1,2,†], Angelo Cipriani[3], Luca Aldega[1], Andrea Billi[4], Eugenio Carminati[1], Roelant Van der Lelij[5], Gianluca Vignaroli[2], and Giulio Viola[2]

[1]*Dipartimento di Scienze della Terra, Sapienza Università di Roma, P.le Aldo Moro 5, Rome, 00185, Italy*
[2]*Dipartimento di Scienze Biologiche, Geologiche ed Ambientali—BiGeA, Università degli studi di Bologna, Via Zamboni 67, Bologna, 40126, Italy*
[3]*Dipartimento per il Servizio Geologico d'Italia—ISPRA, Via V. Brancati 48-60, Rome, 00144, Italy*
[4]*Consiglio Nazionale delle Ricerche, IGAG, Rome, Italy*
[5]*Geological Survey of Norway, Trondheim, 7491, Norway*

ABSTRACT

The central Apennines are a fold-thrust belt currently affected by post-orogenic extensional seismicity. To constrain the influence that the inherited thrust-related structures exert on the present seismic behavior of the belt, we provide the high-resolution structural and hydraulic characterization of one of the most external exposed thrust fault systems of the central Apennines, the Sibillini Mts. Thrust Front (STF). We integrate structural mapping, multiscale structural analysis, and in situ air permeability on the brittle structural facies of the thrust zone. We also performed K-Ar dating of selected fault rocks to better constrain structural inheritance. The STF is defined by a complex, ~300-m-thick deformation zone involving Meso-Cenozoic marl and limestone that results from the accommodation of both seismic and aseismic slip during shortening. Permeability measurements indicate that the low permeability ($10^{-2} \div 10^{-3}$ D) of the marly rich host rock diminishes within the thrust zone, where the principal slip surfaces and associated S-C structures represent efficient hydraulic barriers (permeability down to ~3×10^{-10} D) to sub-vertical fluid flow. Field data and K-Ar dating indicate that the STF began its evolution ca. 7 Ma (early Messinian). We suggest that the studied thrust zone may represent a barrier for the upward migration of deep fluids at the hypocentral depth of present-day extensional earthquakes. We also speculate on the influence that similar deformation zones may have at depth on the overall regional seismotectonic pattern by causing transient fluid overpressures and, possibly, triggering cyclic extensional earthquakes on normal faults prone to slip while crosscutting the earlier thrust zones (as per a classic fault valve behavior). This mechanism may have controlled the origin of the 2016–2017 central Apennines devastating earthquakes.

1. INTRODUCTION

Thrusts and associated structures have long been known to affect fluid flow in the crust by forming sealing caps and/or traps favoring the accumulation of fluid resources such as groundwater and hydrocarbons (Fig. 1; e.g., Harding and Lowell, 1979; Mitra, 1986, 1990; Ingram et al., 2004; Lacombe et al., 2007). The geochemical signature of veins and mineralizations associated with thrusts is consistent with conceptual models wherein moderately dipping thrust zones may act as barriers to fluid flow and migration, that signature being compatible only with local and limited fluid circulation circuits, without significant contributions from far sources or reservoirs (e.g., Ghisetti et al., 2001; Lacroix et al., 2018; Curzi et al., 2020a). This kind of signature is generally remarkably different from the geochemical signature that is instead typical of veins associated with extensional fault systems. There, a wealth of geochemical data indicates a significant contribution from deeply derived fluids, hence implying effective fluid circulation along the vertical dimension, likely along the faults themselves, particularly during the pre- and co-seismic stage of faulting (Fig. 1; e.g., Agosta and Kirschner, 2003; Uysal et al., 2011; Curzi et al., 2021; Vignaroli et al., 2022).

The sealing behavior of thrusts, which is essentially due to the vertical juxtaposition of rock formations with different permeability properties along moderately dipping fault planes and/or to the intrinsically low permeability of the thrust fault rocks themselves (Fig. 1; e.g., Muñoz-López et al., 2020), can have social and economic relevance given its potential effects on the formation and distribution of economic resources and geological hazards (fault valve behavior). For instance, the subsurface storage of CO_2 or H_2 and the natural or anthropogenic increase of pore pressure at depth are influenced and/or modulated by subsurface permeability barriers and are important challenges to face in the near future in the context of the global energy transition (e.g., H_2 storage; Heinemann et al., 2018; Muhammed et al., 2022) and of mitigation of hazards (CO_2 storage; e.g., Deng et al., 2017; seismic hazard due to increase of subsurface pore pressure; e.g., Sibson and Rowland, 2003; Spiers et al., 2017; Schimmel et al., 2019).

To this end, the study of exhumed thrust zones is crucial as it provides useful insights into their hydraulic behavior at depth, although extrapolating surface data to subsurface conditions may require approximations leading to major uncertainties. In other words, although it may be difficult to correlate results from field outcrops with deep correlatives, outcrop studies are still the only way to generate constraints upon buried rocks.

In this paper, we present the results of a study of the thrust-related deformation zone of

Manuel Curzi https://orcid.org/0000-0002-3430-2512
[†]manuel.curzi@unibo.it

GSA Bulletin; January/February 2024; v. 136; no. 1/2; p. 3–26; https://doi.org/10.1130/B36616.1.
Published online 20 March 2023

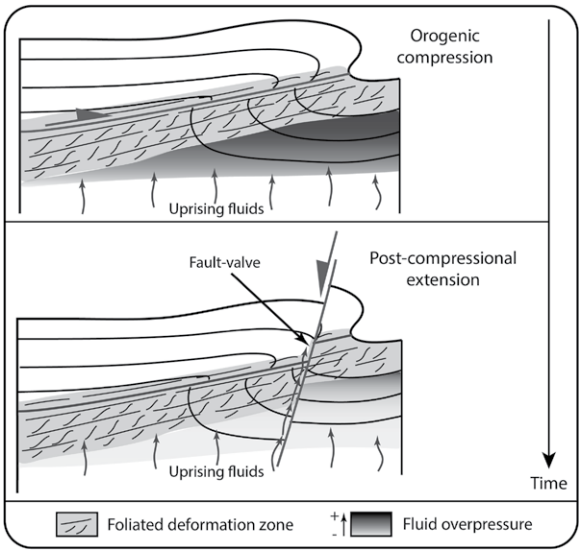

Figure 1. Simplified conceptual model for faulting along post-compressive normal faults that cut and overprint earlier compressional (orogenic) structures in carbonate dominated fold-and-thrust belts. The development of thrust-related highly foliated deformation zones can represent permeability barriers for deep fluids leading to fluid ponding and overpressuring inducing the decreases of the brittle crustal strength and promoting earthquakes during extensional tectonics through the fault-valve behavior.

the Sibillini Mts. Thrust Front (STF), which is a segment of the most external exposed thrust front of the central Apennines of Italy (Calamita and Deiana, 1988; Leoni et al., 2007; Tavani et al., 2012). The STF offers the possibility to investigate the structural architecture, deformation mechanisms, and permeability structure of a remarkable analogue outcrop of buried, compression-related deformation zones in the Apennines that are cut by post-orogenic and seismically-active normal faults. The main aim of this paper is to provide a detailed structural characterization of the STF and to investigate the relationships between structural features and permeability structures at shallow crustal conditions along this fault. In particular, we aim at providing a meso- to microstructural and hydraulic overview of the STF so as to speculate upon its influence on the development of transient fluid overpressure and, possibly, extensional earthquakes along normal faults crosscutting the thrust zone (as per Sibson's fault valve behavior; Sibson, 1981, 1992). To this end, we combined geological mapping and macro- to microscale structural analysis with in situ measurements of rock permeability by air minipermeametry. Based on the obtained results, we speculate on the role that the STF may have played on fluid flow at depth and on the recent extensional seismicity of the central Apennines (e.g., the 2016 Amatrice-Norcia Mw $\leq$ 6.5 seismic sequence; Lavecchia et al., 2016; Chiaraluce et al., 2017). In other words, we speculate upon the role of inherited orogenic structures (i.e., the now inactive thrusts) on present-day seismicity (i.e., post-orogenic extensional earthquakes). Since the studied thrust zone is clay-rich, we also performed K-Ar dating of synkinematic and authigenic clay minerals to better constrain the age of thrusting (e.g., Van der Pluijm et al., 2001; Pană and Van der Pluijm, 2015; Torgersen et al., 2015; Viola et al., 2022). We discuss K-Ar ages in the framework of the Apennines evolutionary history to better constrain structural inheritance as a major factor influencing the ongoing geological evolution of the belt.

2. GEOLOGICAL SETTING

2.1. Central-Northern Apennines

The central-northern Apennines are a NW-SE-striking, E-NE-verging, late Oligocene-to-present fold-and-thrust belt resulting from the convergence and continental collision between Europe and Africa (e.g., Malinverno and Ryan, 1986; Carminati et al., 2010). The structure of the Apennine belt results from the superposition of an early phase of crustal shortening (orogenic compression) and post-compressive extension. This geodynamic evolution has been driven by the progressive retreat of the subducting Adriatic slab toward the east (e.g., Faccenna et al., 2001; Carminati et al., 2012). Compression and extension both began in the inner portion of the belt and progressively migrated eastward toward the Apennine foreland (Cavinato and De Celles, 1999; Billi and Tiberti, 2009; Carminati et al., 2010; Figs. 2A and 2B). In detail, compressive deformation in the central and northern Apennines commenced during the late Oligocene and formed a foreland-verging fold-and-thrust belt (e.g., Patacca et al., 1990; Faccenna et al., 2001; Carminati et al., 2010; Figs. 2A and 2B). Contractional deformation was mainly accommodated by E-NE-verging thrusts that stacked pre- and syn-orogenic successions (e.g., Cosentino et al., 2010; Figs. 2A and 2B). Pre-orogenic successions consist of Upper Triassic-middle Miocene carbonates deposited on a rifted passive margin belonging to the Adria promontory of the Africa Plate (e.g., Cosentino et al., 2010). The syn-orogenic successions consist of upper Miocene siliciclastic sandstone, marl, and shale deposited in foredeep and wedge-top basins (e.g., Pierantoni et al., 2013; Figs. 2A and 2B). Compressional tectonics in the Apennines was strongly influenced by inherited Early Jurassic structures (linked to the Western Tethys rifting) and lateral facies and thickness variations of the sedimentary successions that formed along the Adria margin (Centamore et al., 1971; Calamita, 1990; Santantonio, 1993; Butler and Mazzoli, 2006; Scisciani et al., 2019; Tavarnelli et al., 2019).

Post-compressive and still ongoing extensional deformation in the central-northern Apennines is associated with active NW-SE-striking normal faults, which invariably cut across the earlier contractional (orogenic) structures (e.g., Cosentino et al., 2010; Figs. 2A and 2B). Extensional deformation in the central-northern Apennines began during the middle-late Miocene and is still active, as evidenced by the most recent 2016–2017 Amatrice-Norcia extensional seismic sequence (e.g., Cavinato and De Celles, 1999; Chiaraluce et al., 2017; Curzi et al., 2021; Figs. 2A and 2B). This seismic sequence included the Mw 6.0 Amatrice and Mw 6.5 Norcia mainshocks (Scognamiglio et al., 2016; Chiaraluce et al., 2017; Porreca et al., 2018; Fig. 2A) and caused over 300 casualties and the destruction of many settlements and towns (e.g., Galli et al., 2017). Before the 2016–2017 seismic sequence, many other Mw $\geq$ 6.0 extensional earthquakes had occurred in the central Apennines during histor-

Figure 2. (A) Simplified geological map of the central Apennines showing main thrusts and extensional faults (modified from Curzi et al., 2020a). The Gole dell'Infernaccio and the study area are also shown. (B) Simplified geological cross section of a portion of the central Apennines. Cross-section trace is shown in A. The geological cross section is redrawn from Barchi et al. (2021). (C) Simplified geological map of the Sibillini Mts. in the Gole dell'Infernaccio area (modified from Pierantoni et al., 2013). The portion of the Sibillini Mts. represented in C is shown in A. In C, the point of observation of the panoramic view in Figure 4A and the trace of the schematic cross section (not to scale) in Figure 4B are also shown. (D) Stratigraphic scheme of the Upper Triassic-Miocene succession of the Umbria-Marche-Sabina Domain (modified from Cipriani, 2016).

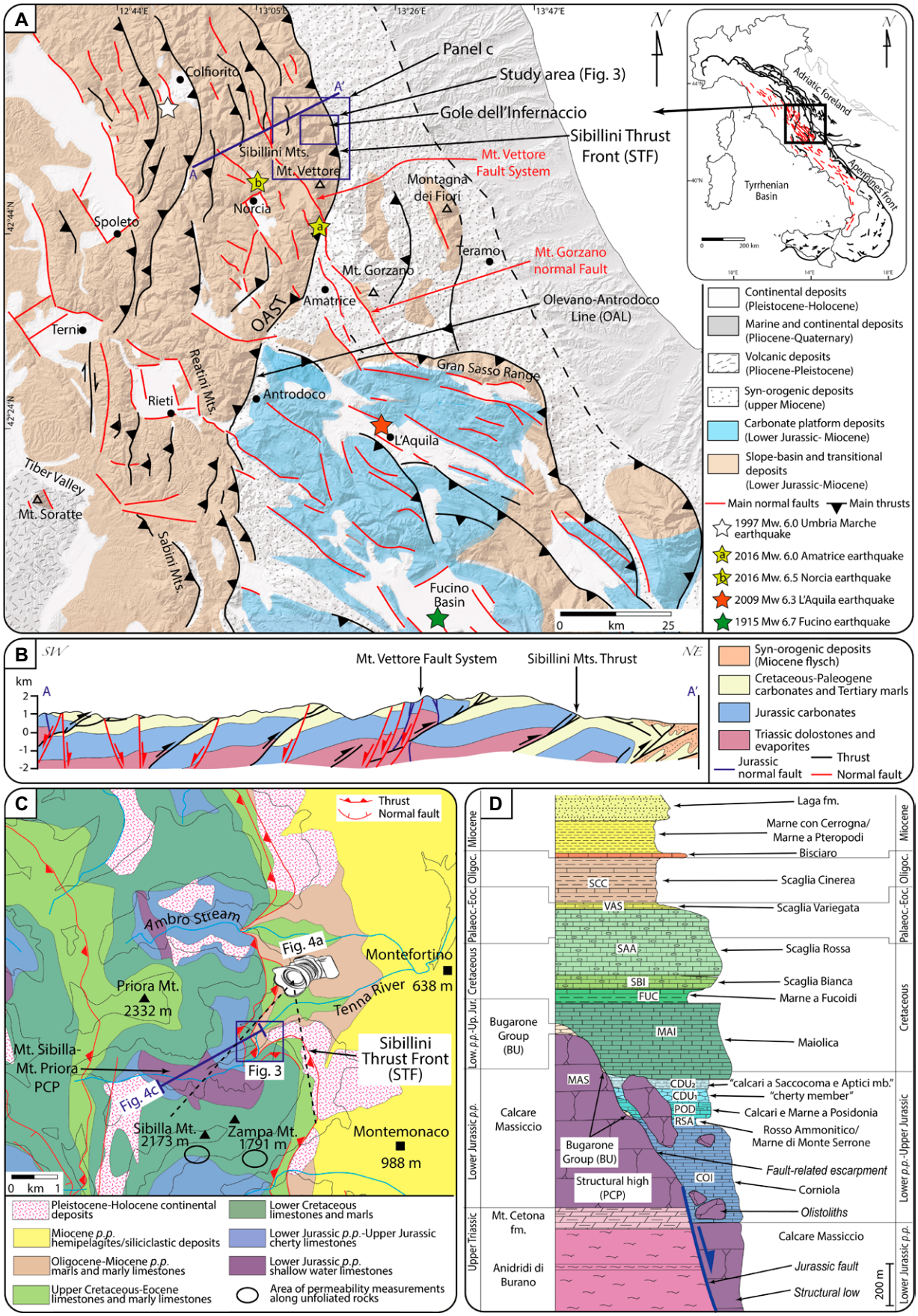

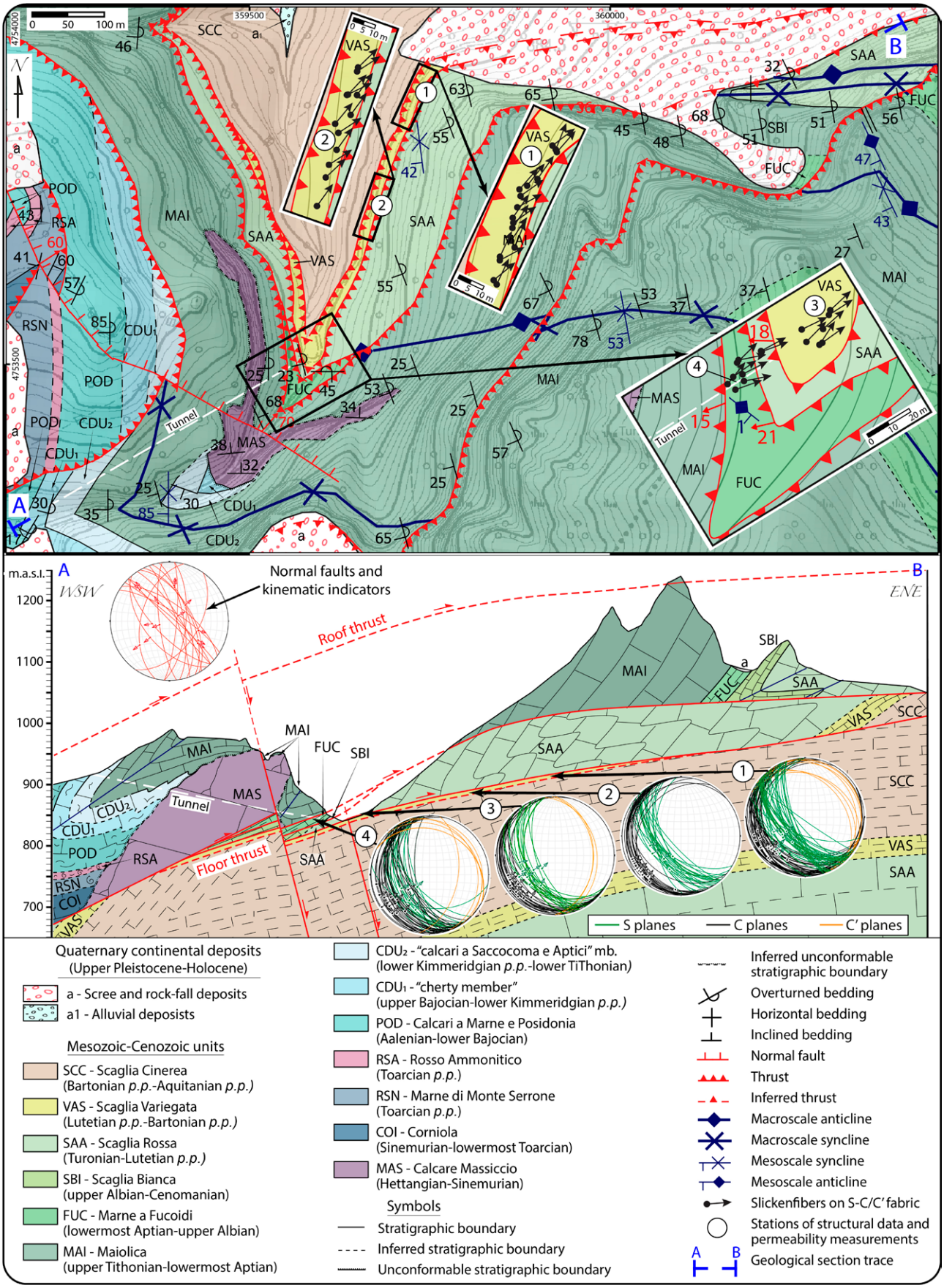

ical and pre-historical times, including the 1639 (MCS intensity 9.5–10) Amatrice earthquake, the 1915 Mw 6.7 Fucino earthquake, the 1997 Umbria Marche seismic sequence (maximum Mw 6.0), and the 2009 Mw 6.3 L'Aquila earthquake (e.g., Galadini and Galli, 2003; Boncio et al., 2004; Miller et al., 2004; Chiarabba et al., 2009; Cinti et al., 2021; Fig. 2A).

2.2. Sibillini Mountains

The Sibillini Mts. are located along the outer front of the central-northern Apennines (known as the Olevano-Antrodoco-Sibillini Thrust, OAST; Fig. 2A), which exhibits a curved shape in map view and can be subdivided into a northern NW-SE-striking frontal segment (Sibillini Thrust Front; STF) and a southern oblique NNE-SSW- to N-S-striking ramp (Olevano-Antrodoco Line, OAL; Fig. 2A; Mazzoli et al., 2005; Pierantoni et al., 2013; Turtù et al., 2013). In particular, the Sibillini Mts. are bordered by the STF to the east and by the OAL to the south and are formed by Mesozoic-Cenozoic rocks of the Umbria-Marche-Sabina Pelagic Basin (UMSPB) sedimentary succession belonging to the Adria passive margin (Centamore et al., 1971; Deiana and Pieruccini, 1971; Chiocchini et al., 1976; Pierantoni et al., 2013; Figs. 2A and 2B). The UMSPB formed during the Early Jurassic rifting stage (e.g., Santantonio and Carminati, 2011; Santantonio et al., 2022). Rifting dissected a Late Triassic-Early Jurassic carbonate platform covered by shallow water carbonates (Anidriti di Burano, "calcari e marne a *Rhaetavicula contorta*"/Mt. Cetona formation and Calcare Massiccio), which, in turn, rest upon a Paleozoic basement. Rifting caused the drowning of the carbonate platform leading to pelagic conditions (e.g., Santantonio and Carminati, 2011). It also led to the development of scattered intra-basinal structural highs (known as pelagic carbonate platforms or PCPs, sensu Santantonio, 1993, 1994; Figs. 2C and 2D) connected with deeper water hanging wall basins by fault-related submarine escarpments. Condensed (up to 50 m thick) pelagic successions (Bugarone Group) formed on the top of the structural highs and locally along paleoescarpments (e.g., Galluzzo and Santantonio, 2002; Fig. 2D). Up to 1.5 km thick marly rich and cherty pelagic deposits accumulated within the hanging wall basins surrounding the PCPs (Corniola, Rosso Ammonitico/Marne di Monte Serrone, Calcari a Marne e Posidonia, and Calcari Diasprigni with its "cherty" and "calcari a Saccocoma e Aptici" members; Fig. 2D). Basin margin successions also host breccias and isolated olistoliths of Calcare Massiccio carbonate sourced from the steep margins of PCPs (Galluzzo and Santantonio, 2002; Pierantoni et al., 2013; Cipriani, 2016, 2019; Cipriani et al., 2020; Fig. 2D).

The study area is located between the Mt. Sibilla-Mt. Priora area, where a complex PCP-basin system was evened out in latest Jurassic-Early Cretaceous by the deposition of the Maiolica limestones (Pierantoni et al., 2013; Cipriani and Bottini, 2019a, 2019b; Cipriani et al., 2019; Fig. 2C). The Marne a Fucoidi, Scaglia Bianca, Scaglia Rossa, Scaglia Variegata, Scaglia Cinerea, Bisciaro, marne con Cerrogna/marne a pteropodi and Laga formations represent the local upper Lower Cretaceous to Neogene marly stratigraphic succession (Pierantoni et al., 2013; Fig. 2D).

This complex Mesozoic-Cenozoic succession was involved in the Apennines orogenic build-up during the late Miocene, when a complex low-angle deformation zone deformed shallow water and pelagic carbonate successions with NE-verging structures (Calamita et al., 1990, 2012; Tavarnelli, 1993; Pierantoni et al., 2013; Pace et al., 2022a, 2022b). Compressional deformation, which locally reactivated, truncated, and rotated pre-thrusting normal faults, was accommodated by thrusts (and associated S-C fabrics) and fault-propagation folds (Tavarnelli, 1993; Tavarnelli et al., 2004; Pizzi and Galadini, 2009; Di Domenica, 2012; Pierantoni et al., 2013; Pace and Calamita, 2014; Pace et al., 2015, 2022a; Calamita et al., 2018). The latter are locally characterized by box-shape interpreted by some authors as being associated with blind thrusts (in turn interpreted as inherited Jurassic normal fault segments passively rotated and reactivated during shortening; e.g., Cooper and Burbi, 1986; Calamita, 1990; Pierantoni et al., 2013; Pace et al., 2022a). Compressional deformation was followed by extensional tectonics, which began during Pleistocene-Holocene times and is still ongoing (e.g., Galadini and Galli, 2003; Stendardi et al., 2020). Extensional tectonics, which locally reactivated pre-thrusting normal faults (e.g., Pizzi et al., 2017; Porreca et al., 2020), produced NW-SE-striking normal fault systems in the area (Mt. Vettore Fault System and Mt. Gorzano normal Fault), which cut the STF (Galadini and Galli, 2003; Stendardi et al., 2020; Figs. 2A and 2B) and are still seismically active (Lavecchia et al., 2016; Chiaraluce et al., 2017).

Figure 3. Geological-structural map and geological cross section of the Sibillini Thrust Front (STF) in the Gole dell'Infernaccio area (see Figs. 2A and 2C for location). The sites of the structural stations are shown as are shown also the Schmidt nets (lower hemisphere projection) of attitudes of S-C/C' tectonites, normal faults, and related kinematic indicators (calcite slickenfibers). Note that part of the cross section was built based on data and observations from rock exposures in a tunnel (see text for further information), whose trace (white dashed line) is shown in the map (above).

3. MATERIAL AND METHODS

To reconstruct the deformation history of the study area, its mechanical and permeability properties, and to radiometrically constrain the age of compression, we combined different analytical techniques including:

(1) Detailed geological-structural mapping at the 1:5,000 scale of an area of ~2 km^2 to reconstruct the surface and subsurface geometries. The detailed geological mapping forms the basis for the meso-structural analysis of key exposures to reconstruct the architecture of the deformation zone and for the well-informed sampling strategy followed to select the most representative samples.

(2) Detailed meso-structural analysis and related collection of representative rock samples. In particular, we focused our observations on localized and distributed deformation structures and marly rich fault rocks.

(3) Microstructural analysis of fault rocks by means of a high-resolution scanner and optical microscopy to infer the deformation mechanisms and qualitative permeability properties.

(4) In situ air permeability within the deformation zone (i.e., parallel and orthogonal both to the thrust principal slip surfaces and tectonic foliation) and away from the deformation zone to assess eventual permeability changes associated with tectonic anisotropies.

(5) X-ray diffraction (XRD) analysis of fault gouge samples to define their mineralogical assemblage. This analysis was mainly complementary to K-Ar dating.

(6) K-Ar geochronology of authigenic and syn-kinematic clay minerals from two fault gouge samples to constrain the timing of thrusting and development of the deformation zone.

Analytical techniques are fully described in the Supplemental Material.

Where not specified, the lithostratigraphic units reported in this work are formation-rank traditional units (Cita et al., 2007a, 2007b).

4. RESULTS

4.1. First-Order Structural Framework of the STF

The STF in the study area is characterized by a ~300-m-thick duplex formed by four horses bounded by NE-verging thrusts (Figs. 3, 4A, and 4C). In the hanging wall of

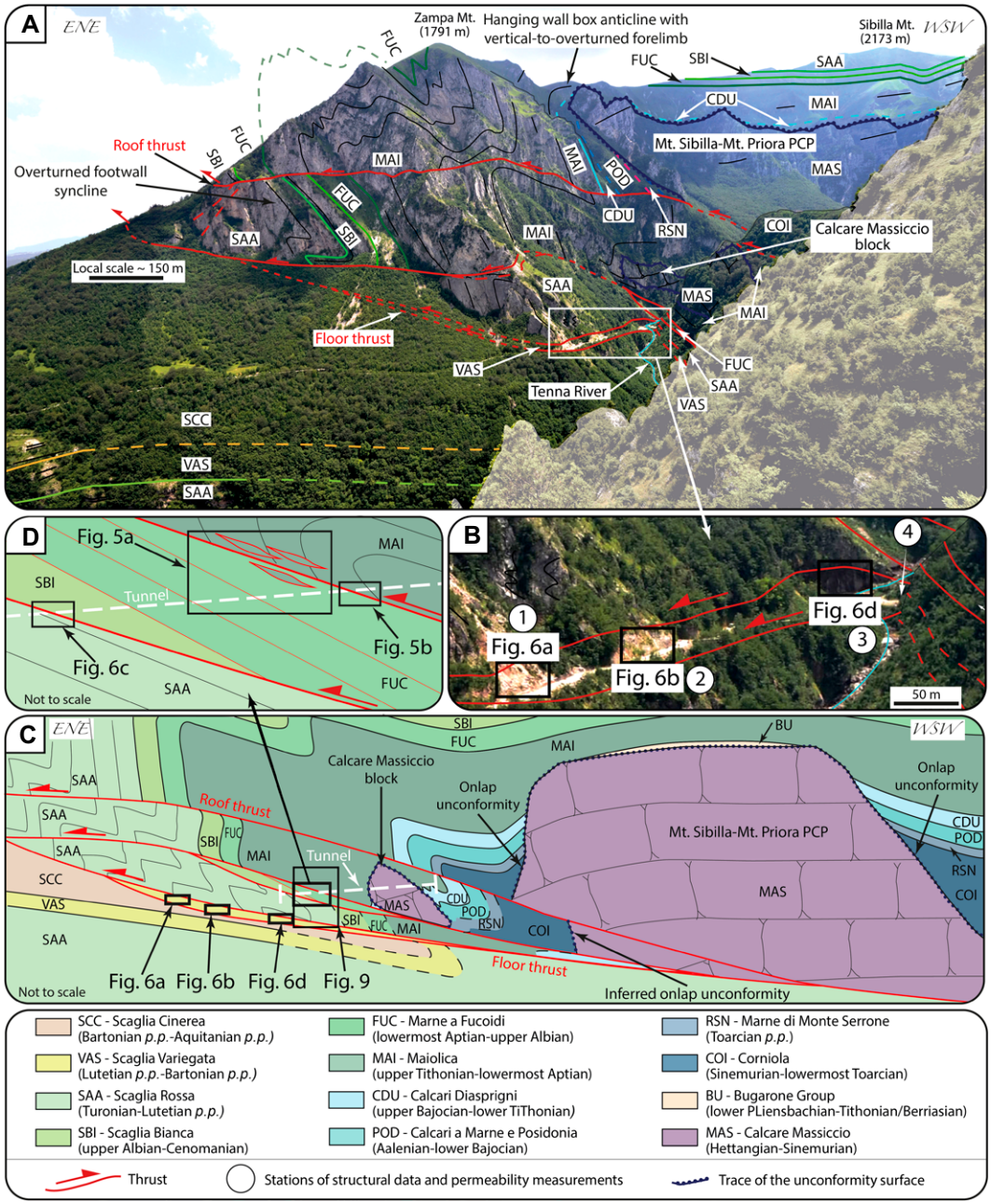

Figure 4. (A) Panoramic view (from NW) of the Gole dell'Infernaccio area with geological interpretation and location of some studied outcrops. Note the roof and floor thrusts which bound a ~300-m-thick deformation zone is made up of four horses involving Mesozoic-Cenozoic carbonates. The observation point of the panoramic view is shown in Figure 2C. (B) Detail of the valley floor where the lower horse is exposed and the structural stations 1–3 are located. The structural station 4 is located within the tunnel. (C) Schematic cross section (not to scale) showing the geology of the Gole dell'Infernaccio area. The trace of the tunnel and the location of some studied outcrops are shown. The trace of the section, which runs along the tunnel and valley floor, is shown in Figure 2C. (D) Schematic detail of two SW-dipping and NE-verging thrusts exposed in the tunnel, where the structural station 4 is located.

the main roof thrust there occurs a box anticline with a sub-horizontal western backlimb and a vertical to overturned eastern forelimb (Figs. 4A and 4C). The Jurassic core of the anticline is formed by the Mt. Sibilla-Mt. Priora Jurassic PCP-basin system (Calcare Massiccio, PCP-top Bugarone Group, and basin-fill succession onlapping the PCP margins; Figs. 2C, 4A, and 4C).

The structurally highest horse (i.e., that bounded above by the main roof thrust) is up to ~250 m thick and is composed of a partially overturned Upper Jurassic to Upper Cretaceous succession (Fig. 4C). Its more internal exposed portion is characterized in the west by an ENE-verging syncline with an overturned western limb deforming Middle Jurassic-lowermost Cretaceous pelagites (from Calcari e Marne a Posidonia to Maiolica carbonates; Figs. 2C and 4C) onlapping and burying in the east a Calcare Massiccio block (Figs. 3, 4A, and 4C). The syncline is associated with lower-order mesoscopic folds affecting the "calcari a Saccocoma e Aptici" and Maiolica marly and cherty limestone (Figs. 2C, 3, 4A, and 4C). The exposed portion of the underlying horse is represented by ~30 m of delaminated and overturned Marne a Fucoidi and Scaglia Bianca marl and limestone (Figs. 3 and 4C). The exposed portions of the two structurally lowest horses contain ~20 m of delaminated and overturned Scaglia Rossa and Scaglia Variegata marly limestone (Figs. 3 and 4C). The footwall of the STF is represented by the gently W-dipping Oligocene marl of the Scaglia Cinerea (Fig. 4A).

NW-SE-striking, NE-dipping normal and oblique faults with a maximum displacement of 40–50 m cut the stacked structures (Fig. 3).

4.2. Meso- and Microscopic Structural Analysis of the STF

We studied in detail some representative outcrops within the STF deformation zone (Figs. 3 and 4B–4D). Most outcrops are continuously

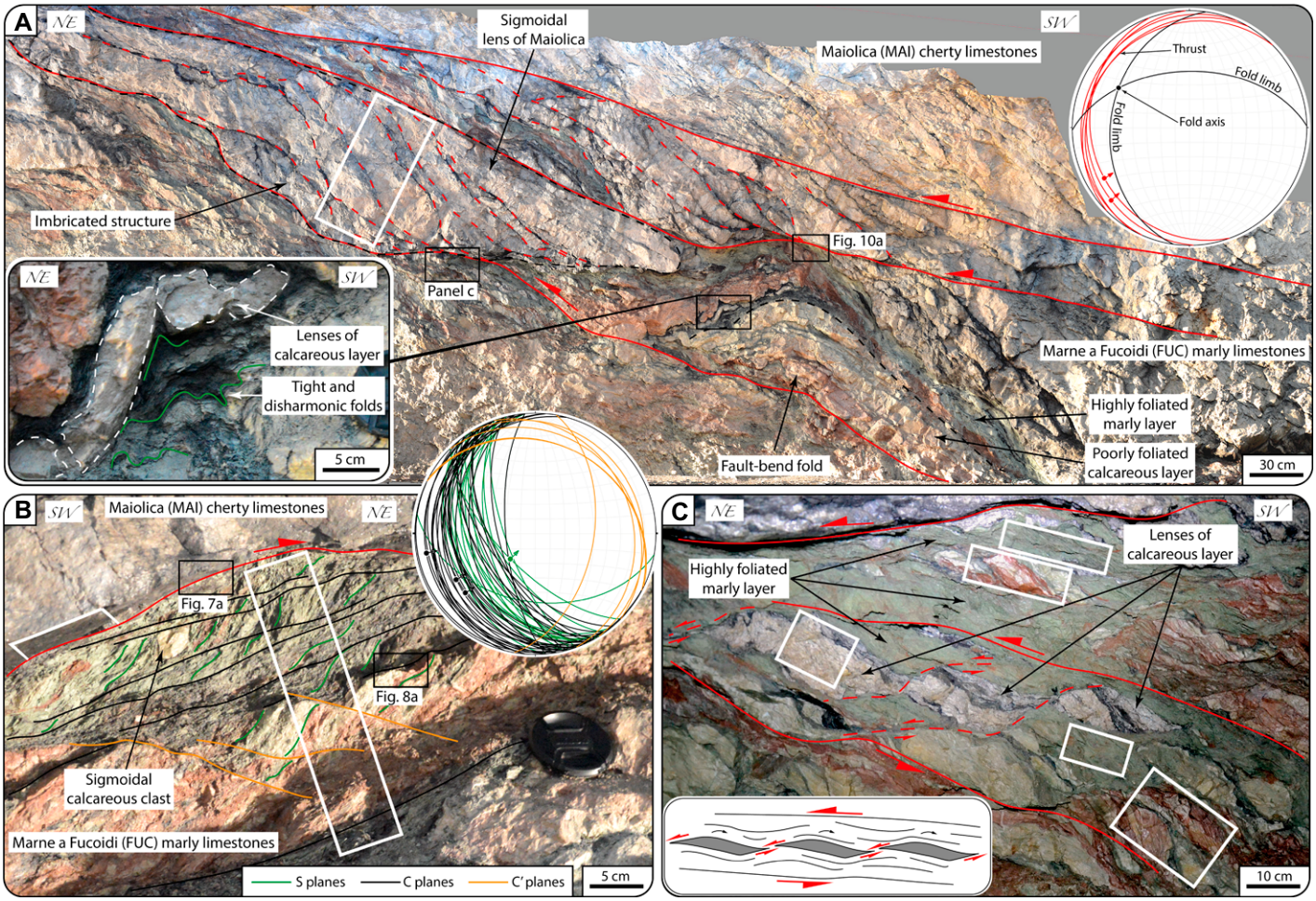

Figure 5. Photos from the tunnel in the Gole dell'Infernaccio. (A) Tectonic contact between the structurally highest and the underlying horses (structural site no. 4; see Figs. 3 and 4 for location). The contact is represented by three SW-dipping, NE-verging thrusts, which juxtapose the Maiolica limestones onto the Marne a Fucoidi marls and marly limestones. The Maiolica cherty limestones form metric sigmoidal lenses characterized by an internal structure imbricated toward the NE. The Marne a Fucoidi pelagites exhibit highly (marly) and poorly (calcareous) foliated domains. Note a NW-plunging fault-bend fold above the lower thrust. Inset in A shows the detail of the northern (left) fold limb along which laterally segmented layers are embedded within a highly foliated domain, which exhibits centimetric tight and disharmonic folds. Schmidt net (lower hemisphere projection) shows attitude of thrusts (with related kinematic indicators), fold limbs, and fold axis. (B) S-C/C' tectonites within the foliated (marly) domain of the Marne a Fucoidi. (C) Asymmetric calcareous lenses embedded within the highly foliated (marly) domain of the Marne a Fucoidi. The shape of the lenses is consistent with shear-induced back-rotation. See in C a schematic representation of the typical sense of back-rotation of shear-band deformed lenses. The white rectangles represent the areas where in situ air permeability measurements have been carried out.

exposed in a tunnel (Fig. S1[1]). Along the structurally highest horse, the pelagic chert and marl of the "calcari a Saccocoma e Aptici" onlapping the Calcare Massiccio block are characterized by mesoscopic, tight and disharmonic folds with SW-dipping to sub-vertical axial planes (Figs. 4C).

The contact between the highest horse and the underlying horses is marked by three SW-dipping and NE-verging thrusts that juxtapose the Maiolica cherty limestone on top against the Marne a Fucoidi marly limestone (Figs. 4C, 4D, and 5A). A metric fault-bend fold occurs within the Marne a Fucoidi marly limestone and is characterized by a SW-dipping (~25°) limb and a steeper NE-dipping limb (~45°; Fig. 5A). The fold axis plunges ~20° to the SE (Fig. 5A). Along the NE-dipping limb, lenses of carbonates are embedded within foliated marly domains deformed by centimetric, tight and disharmonic folds (Fig. 5A). The marly layers of the Marne a Fucoidi marly limestone are pervasively foliated to form S-C/C' tectonites with closely spaced S planes (~0.2 cm), C planes (~1 cm), and C' planes (~2 cm; Fig. 5B). The S-C/C' tectonites are compatible with a top-to-NE sense of shear, as also indicated by centimetric sigmoidal calcareous clasts (Fig. 5B). Within the S-C/C' tectonites, high aspect-ratio asymmetric calcareous lenses compatible with shear-induced back-rotation are also observed (Fig. 5C). The Maiolica cherty limestone

[1]Supplemental Material. Supplemental Text: Methods. Figure S1. Figure S2: X-ray diffraction patterns for randomly oriented mounts for the different grain-size fractions of sample GI12 with reflections of illite polytypes. Table S1: Summary of in situ permeability measurements both within and outside the deformation zone. Table S2: K-Ar data for the gouge samples of the Sibillini Mts. Thrust. Please visit https://doi.org/10.1130/GSAB.S.21821781 to access the supplemental material, and contact editing@geosociety.org with any questions.

is characterized by metric sigmoidal lenses embedded within the highly foliated Marne a Fucoidi marly limestone (Fig. 5A). The sigmoidal lenses belong to a structure imbricated toward the NE (Fig. 5A).

Within the two lowest horses (Figs. 3 and 4C), pervasive S-C/C' tectonites constraining a top-to-NE reverse sense of shear are observed and are particularly pervasive within the Scaglia Variegata marly limestone (Figs. 3, 6A, and 6B). The S-C/C' tectonites are invariably characterized by NW-SE-striking and WSW-dipping (10°–65°) solution planes (Figs. 3, 6A, and 6B). These S planes bear calcite slickenfibers along the pressure-solution surfaces (compatible with a top-to-NE sense of shear), indicating that these structures first developed in response to pressure-solution and were subsequently exploited to localize shearing at a later stage (see Schmidt diagram in Figs. 3, 6A, and 6B). C planes strike NNW-SSE, dip 2°–30° toward the WSW, and bear calcite slickenfibers indicating a top-to-NE sense of shear (see Schmidt diagram in Figs. 3, 6A, and 6B). C' planes are less common, strike NW-SE, and dip mainly to the NE (5°–25°; see Schmidt diagram in Figs. 3, 6A, and 6B). Gently NE-dipping (5°–20°) and low-displacement (up to ~50 cm) back-thrusts accommodating a top-to-SW sense of shear are seldom observed (Fig. 6A). The backthrust surfaces localize along bedding surfaces and locally cut across bedding (Fig. 6A). Flame-like tectonic structures are observed within the Scaglia Variegata marly limestone and are outlined by metric decolorized bands with an irregular shape (Fig. 6B).

Low-displacement (up to ~1 m) NE- or SW-dipping (50°–90°) as well as ESE- or WNW-dipping (40°–60°) conjugate normal or oblique faults cut across the deformation zone. Along the poorly foliated domains of the STF deformation zone, normal faults are represented by discrete brittle surfaces (Fig. 6C). Within the portions of the deformation zone containing top-to-NE S-C/C' tectonites, up to 30-cm-thick extensional shear zones characterized by dragged and rotated S-C/C' tectonites are locally observed (Fig. 6D).

To better constrain the deformation mechanisms active during faulting along the STF, we analyzed numerous thin sections of Maiolica cherty limestone and Marne a Fucoidi marly limestone from within the deformation zone. The principal slip surface (PSS) between the Maiolica cherty limestone (in the hanging wall) and the Marne a Fucoidi marly limestone (in the footwall; Figs. 5 and 7A) is ~1 mm thick and is decorated by insoluble material, which locally represents the matrix of a very fine-grained cataclasite composed of ~400 μm thick fragments of calcite veins and host rock (Figs. 7A and 7B).

The Maiolica cherty limestone-derived rocks in the immediate hanging wall above the PSS consists of foliated cataclasite with micrometric to centimetric fragments of reworked calcite veins and calcareous and cherty clasts (Fig. 7A). Foliation therein is parallel to the PSS and is defined by gently undulated, 0.5–1 cm spaced and teeth-shaped solution planes (Fig. 7A). The calcareous and cherty clasts are internally brecciated and contain variably oriented micrometric calcite veins (Fig. 7A). Chert clasts are also brecciated to form angular fragments within a calcite cement with a blocky texture (Figs. 7B and 7C).

The Marne a Fucoidi rocks in the footwall below the PSS are sheared by pervasive S-C tectonites (Figs. 8A and 8B) tightly juxtaposing microdomains with relatively different rheology. The more competent microdomains are characterized by up to ~700 μm spaced S planes and are crosscut by orthogonal, up to ~200-μm-thick calcite veins (Fig. 8B). Calcite veins are, in turn, also cut across and locally presso-soluted by S planes preserving evidence of localized dissolution (Fig. 8B).

The intermediate competence microdomains are characterized by closely spaced (very few microns) and anastomosed S planes, which are locally amalgamated to form up to ~1 cm thick bands of insoluble material (Figs. 8A, 8C, and 8D). S planes also surround planktonic foraminifera, which are preserved or only partially dissolved by S planes, therefore representing pinning barriers at the microscale (Fig. 8D). Blocky and elongated-blocky calcite veins are arranged parallel to S planes (i.e., orthogonal to the maximum stress orientation inferred by the S plane attitude) and are locally bounded by both scabrous (teeth-shaped) solution planes as well as by sharp planes (Fig. 8D). Furthermore, between such scabrous solution planes and sharp planes, up to ~15-μm-thick en-échelon calcite veins are also observed (Fig. 8D). The calcite veins parallel to the S planes are also included and sheared between solution planes and form sigmoidal lenses locally accommodated by synthetic micrometric shear planes (C' planes; Fig. 8D).

The less competent microdomains of the S-C tectonites are represented by organic matter-rich levels (especially observable within the Marne a Fucoidi marly limestones). These domains are characterized by sub-horizontal S planes (parallel to C planes), which are closely spaced and systematically amalgamated, forming bands of insoluble material (Figs. 8A and 8C). These bands are anastomosed and surround sigmoidal micrometric calcareous blocks, within which micrometric calcite veins occur (Fig. 8C). The contacts between the less and the more competent microdomains are defined by sheared calcite veins (Fig. 8C). Furthermore, lenses of calcareous blocks (containing calcite veins and pressure solution planes) are enveloped by hooked and curved bands of insoluble material (Fig. 8C) attesting to local shear-induced vorticity (rotation of lenses of calcareous block within the softer bands of insoluble material).

4.3. In situ Air Permeametry Results

In situ permeametry was carried out both within and far (~2 km) from the deformation zone (Fig. 9A). Results are listed in Table S1 and shown in Figure 9B. Permeability measurements from outside the deformation zone (see Fig. 2C for location) were collected both parallel and perpendicular to the bedding (S_0) of the Maiolica cherty limestone, Marne a Fucoidi marly limestone, and Scaglia Rossa marly limestone. As a whole, the permeability parallel and orthogonal to the bedding of the analyzed lithotypes vary between $\sim 6 \times 10^{-1}$ and $\sim 7 \times 10^{-5}$ and from $\sim 7 \times 10^{-1}$ to $\sim 6 \times 10^{-5}$ D, respectively (Fig. 9B). Permeability parallel to bedding has mean values between $\sim 6 \times 10^{-2}$ and $\sim 2 \times 10^{-2}$ D and is up to one order of magnitude higher than orthogonal to bedding (with mean values between $\sim 6 \times 10^{-2}$ and $\sim 7 \times 10^{-3}$ D; Fig. 9B).

Figure 6. (A) Scaglia Variegata marly limestones (structural site no. 1; see Figs. 3 and 4 for location) characterized by S-C/C' tectonites indicating a top-to-NE sense of shear. A small-displacement (~50 cm) backthrust with a top-to-SW sense of shear is also shown. (B) Scaglia Variegata marly limestones (structural site no. 2; see Figs. 3 and 4 for location) characterized by flame tectonic structures outlined by metric decolorized bands with an irregular shape and by S-C/C' tectonites indicating a top-to-NE sense of shear. (C) Small displacement (~25 cm) normal faults cutting the thrust surfaces which juxtapose the Scaglia Bianca limestones onto the Scaglia Rossa deposits (intermediate horses). (D) Compressional deformation zone showing top-to-NE S-C/C' tectonites cut by an up to 30 cm thick extensional deformation zone. The extensional deformation zones are bounded by normal faults and are characterized by dragged and rotated S-C/C' tectonites. Note the dragged S-C/C' tectonites at the footwall of the extensional faults which bound the extensional deformation zones. The white rectangles represent the areas where in situ air permeability measurements have been carried out.

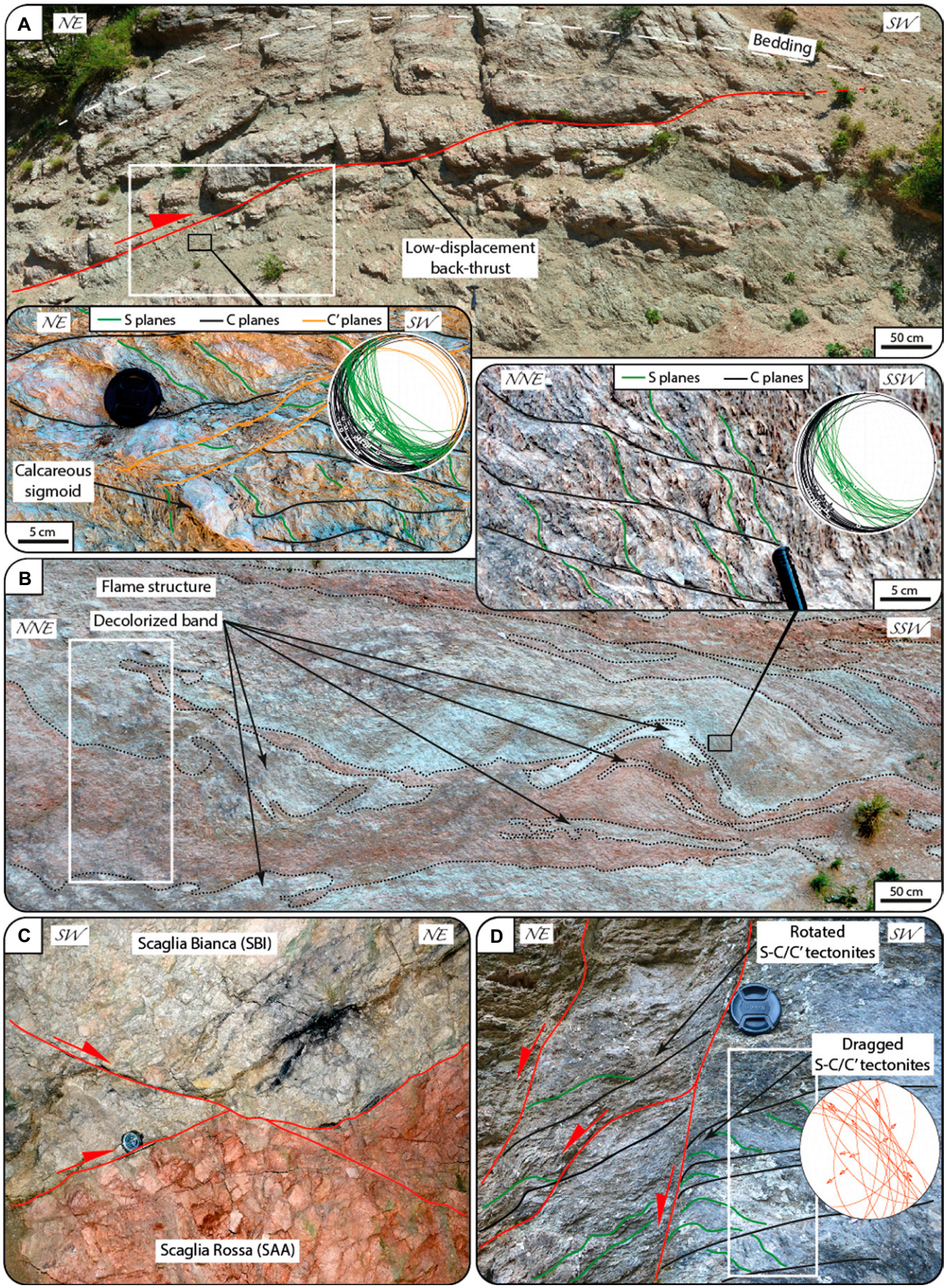

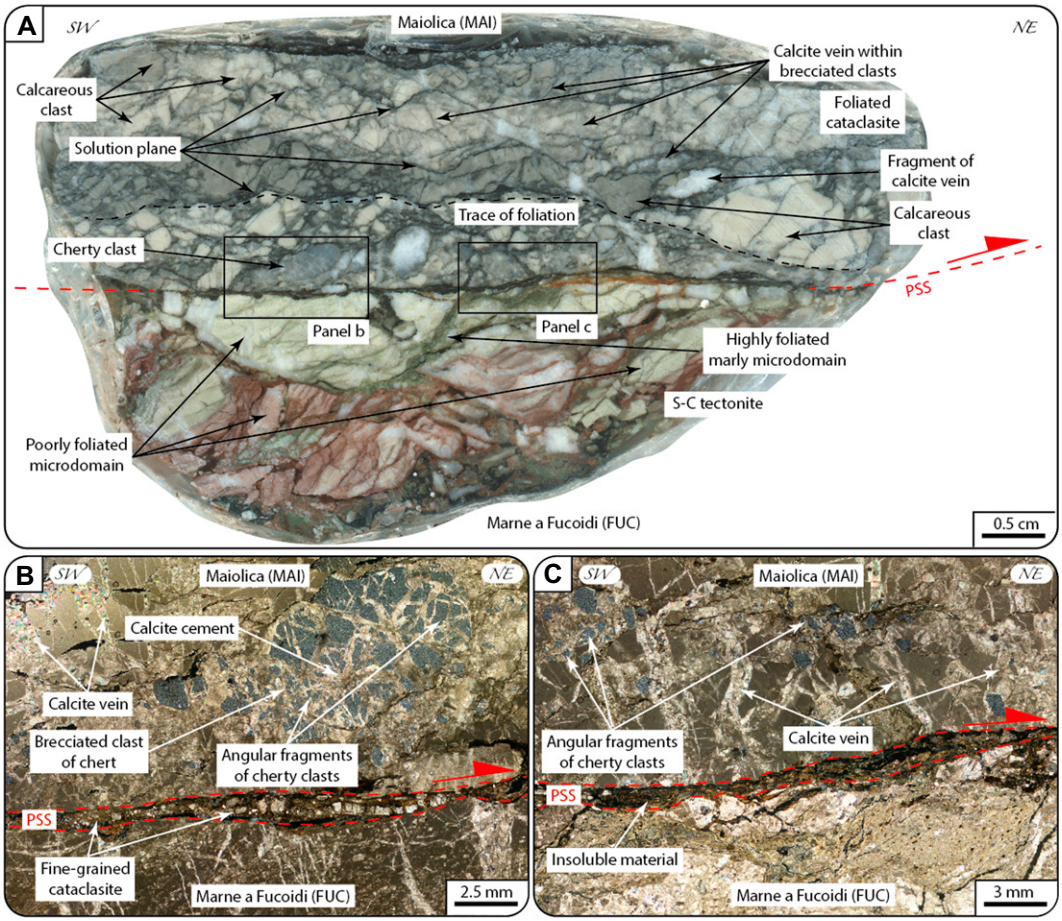

Figure 7. (A) High-resolution scan image of the principal slip surface (PSS) between Maiolica cherty limestones (in the hanging wall) and the Marne a Fucoidi marly limestones (in the footwall; see Fig. 5B). This image includes both hanging wall and footwall rocks. The Maiolica cherty limestone consists of foliated cataclasite with micrometric to centimetric fragments of reworked calcite veins, calcareous clasts, and cherty clasts. The foliation, marked by widely spaced dissolution planes (dashed black lines), is parallel to the PSS (dashed red line). (B) Detail of the PSS and hanging wall rocks. Notice that the PSS is composed of insoluble material, which locally represents the matrix of a very fine-grained cataclasite composed of ~400-µm-thick fragments of calcite veins and host rocks. Also notice the angular fragments of brecciated cherty clasts embedded within blocky calcite cement in the hanging wall rocks. (C) Detail of the PSS and hanging wall rocks. Notice the insoluble material along the PSS, the calcite veins, and the angular fragments of cherty clasts within the hanging wall rocks.

The permeability within the thrust deformation zone has been measured (1) perpendicular to the PSS juxtaposing the Maiolica cherty limestone onto the Marne a Fucoidi marly limestone, (2) both parallel and perpendicular to the S-C tectonites, and (3) parallel to the foliation within calcareous lenses embedded within the S-C tectonites (Fig. 9A). The permeability parallel to the S-C tectonites exposed within the Scaglia Variegata marly limestone (structural stations 1, 2, and 3; Figs. 3, 6A, 6B, 6C, and 9A) ranges between ~5 and ~10^{-2} D and is up to five orders of magnitude higher than that measured orthogonally to S-C tectonites, which is characterized by values between ~3×10^{-1} and ~3×10^{-5} D (below the actual reliability limit of the utilized air-minipermeameter; Fig. 9B). The mean permeability values measured parallel and orthogonal to the S-C tectonites range from ~2 to ~2×10^{-1} D and from ~8×10^{-3} to ~2×10^{-3} D, respectively (Fig. 9B). The mean permeability parallel and orthogonal to the S-C tectonites exposed within the Marne a Fucoidi marly limestone (structural station 4; Figs. 3, 5B, 5C, and 9A) is between ~1×10^{-1} and ~6×10^{-2} D, respectively (Fig. 9B). The permeability within the lenses of calcareous layers embedded within the Marne a Fucoidi marly limestone (Figs. 5C and 9A) ranges from ~4×10^{-1} to ~9×10^{-5} D and has a mean value of ~5×10^{-2} D (Fig. 9B).

The permeability orthogonal to the PSS between Maiolica and Marne a Fucoidi marly limestones (Figs. 5A and 9A) has the lowest minimum value (~3×10^{-5} D), spans from ~7×10^{-1} to ~3×10^{-5} D, and has a mean value of ~6×10^{-2} D (Fig. 9B).

4.4. X-Ray Diffraction of the Dated Fault Gouge

We analyzed two samples (GI11 and GI12) of fault gouge along the thrust surface juxtaposing the Maiolica limestones in the hanging wall against the Marne a Fucoidi marl in the footwall (structural site no. 4; Figs. 3–5). The gouge, formed at the expense of the Marne a Fucoidi marls, was separated into five grain size fractions (<0.1 µm, 0.1–0.4 µm, 0.4–2 µm, 2–6 µm, and 6–10 µm; Fig. 10A). The mineralogical assemblage consists of quartz, K-feldspar, albite, calcite, illite-2M_1, illite-1 M, and chlorite. Quartz is present in each subfraction and ranges between 11% and 37%. K-feldspar and albite ranges between 1%–2% and 7% and are absent in the finest fraction of each sample. A general and progressive decrease in calcite content is evident from the coarsest to the finest fractions (Fig. 10A). Illite-2M_1 generally increases from the coarsest (6–10 µm) to the finest (<0.1 µm) fractions (from 18% to 32% in the sample GI11 and from 11% to 35% in the sample GI12). Illite-1 M is absent in the 2–6 µm and 6–10 µm fractions and increases from 8% to 52% in the sample GI11 and from 8% to 49% in sample GI12 toward the finest fractions. In the histograms of Figure 11A, we report the relative abundance of 2M_1 and 1 M illite normalized to 100% that have been used for the illite age analysis (IAA; see the following section). Chlorite does not exceed 2% and it is absent in the <0.1 µm and 0.1–0.4 µm fractions.

4.5. K-Ar Geochronology

The five grain size fractions (<0.1 µm, 0.1–0.4 µm, 0.4–2 µm, 2–6 µm, and 6–10 µm) separated from the two samples of fault gouge

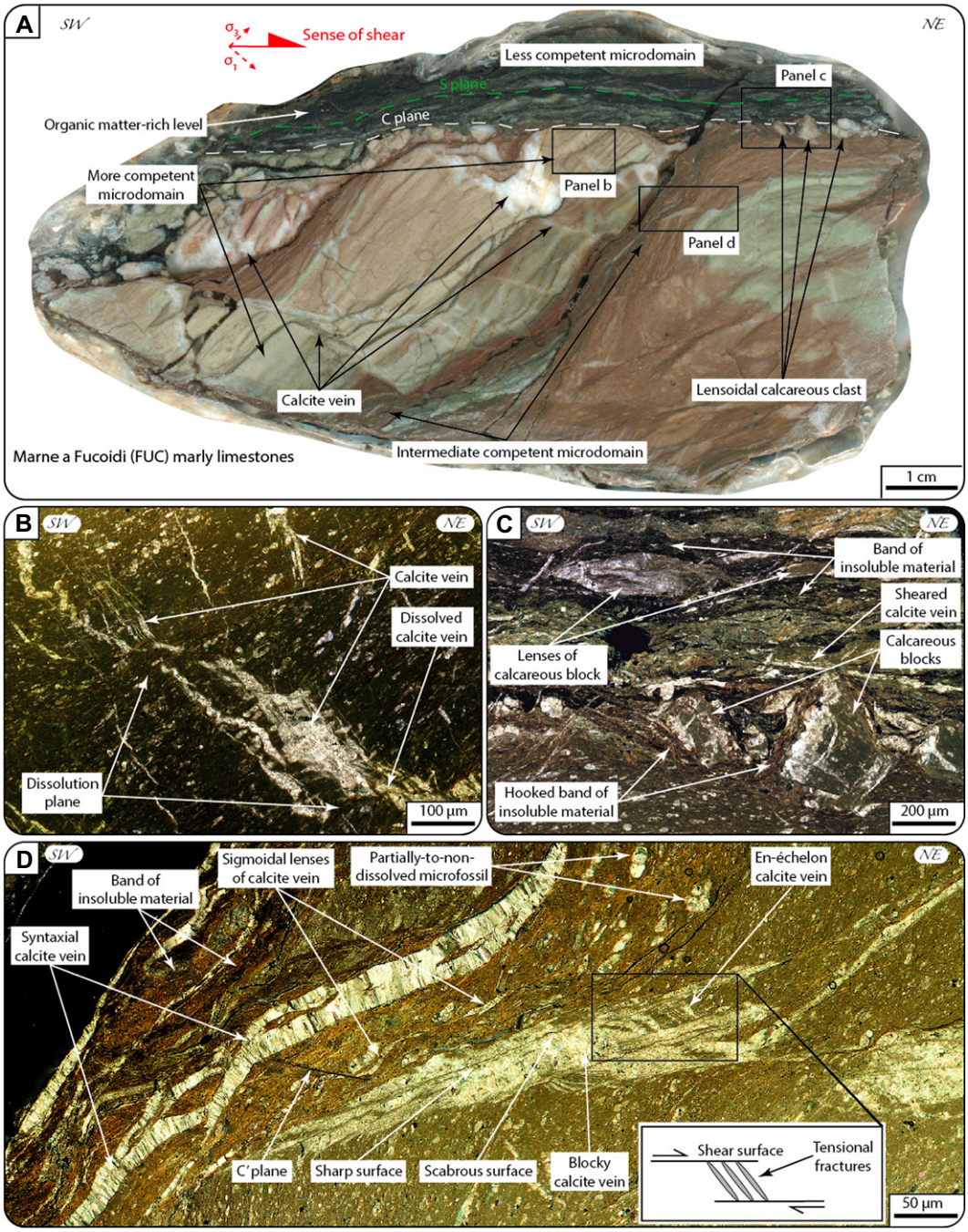

Figure 8. (A) High-resolution scan image of the foliated Marne a Fucoidi marly limestones with a pervasive S-C/C' fabric (see Fig. 5B for location). Note the presence of microdomains with different styles of deformation marked by the different spacing of dissolution S planes. (B) Detail of the poorly foliated microdomain, characterized by spaced (up to ~700 µm) solution S planes and crossed by up to ~200-µm-thick calcite veins oriented orthogonal to the S planes. Calcite veins are cut and dissolved by solution S planes. (C) Detail of the less competent microdomain, represented by organic matter-rich levels, characterized by sub-horizontal (parallel to the principal slip surface) amalgamated S planes forming bands of insoluble material. The boundary between the less competent microdomain and the more- or intermediate-competent microdomain is represented by shear C planes marked by sheared calcite veins. Along such planes, lensoidal calcareous blocks are also present. (D) Detail of the intermediate competent microdomain characterized by closely spaced (few microns) and anastomosed S planes, which locally forms bands of insoluble material. Planktonic foraminifera are preserved or only partially reworked. Blocky and elongate-blocky calcite veins are arranged parallel to the S planes and are bounded by both scabrous (teeth-shaped) solution planes and sharp planes. Between the shear planes and parallel to the S planes, up to ~15-µm-thick en-échelon calcite veins are present. See in D a schematic representation of the development of the observed en-échelon calcite veins.

(samples GI11 and GI12; Fig. 10B) have been dated by K-Ar isotopic dating (Table S2). For all the samples, dates define an inclined spectrum (sensu Pevear, 1999), wherein the coarsest fraction yields the oldest age and the finest fraction the youngest age (Fig. 10B). Ages of the intermediate size subfractions decrease with the grain size between these two end members (Fig. 10B). In detail, from the coarsest to the finest fractions, sample GI11 yields K-Ar dates between 160 ± 2.2 Ma (Late Jurassic) and 64 ± 0.9 Ma (early Paleocene; Fig. 10B), and sample GI12 yields K-Ar dates between 160.1 ± 0.9 Ma (Late Jurassic) and 65 ± 0.9 Ma (early Paleocene; Fig. 10B). The ages of the three coarsest fractions, older than the stratigraphic age of the host rock (Aptian-Albian; Fig. 10B), as well as the ages of the finest fraction, younger than the stratigraphic age of the host rock, suggest mixing between authigenic and detrital illite inherited from the host rock (Aldega et al., 2019; Carboni et al., 2020; Curzi et al., 2020a). In this context, to derive geologically meaningful results, we assessed the effects of host rock contamination by detrital illite by the Illite Age Analysis approach (IAA; Pevear, 1999). In detail, to estimate the age (and associated uncertainty) of the

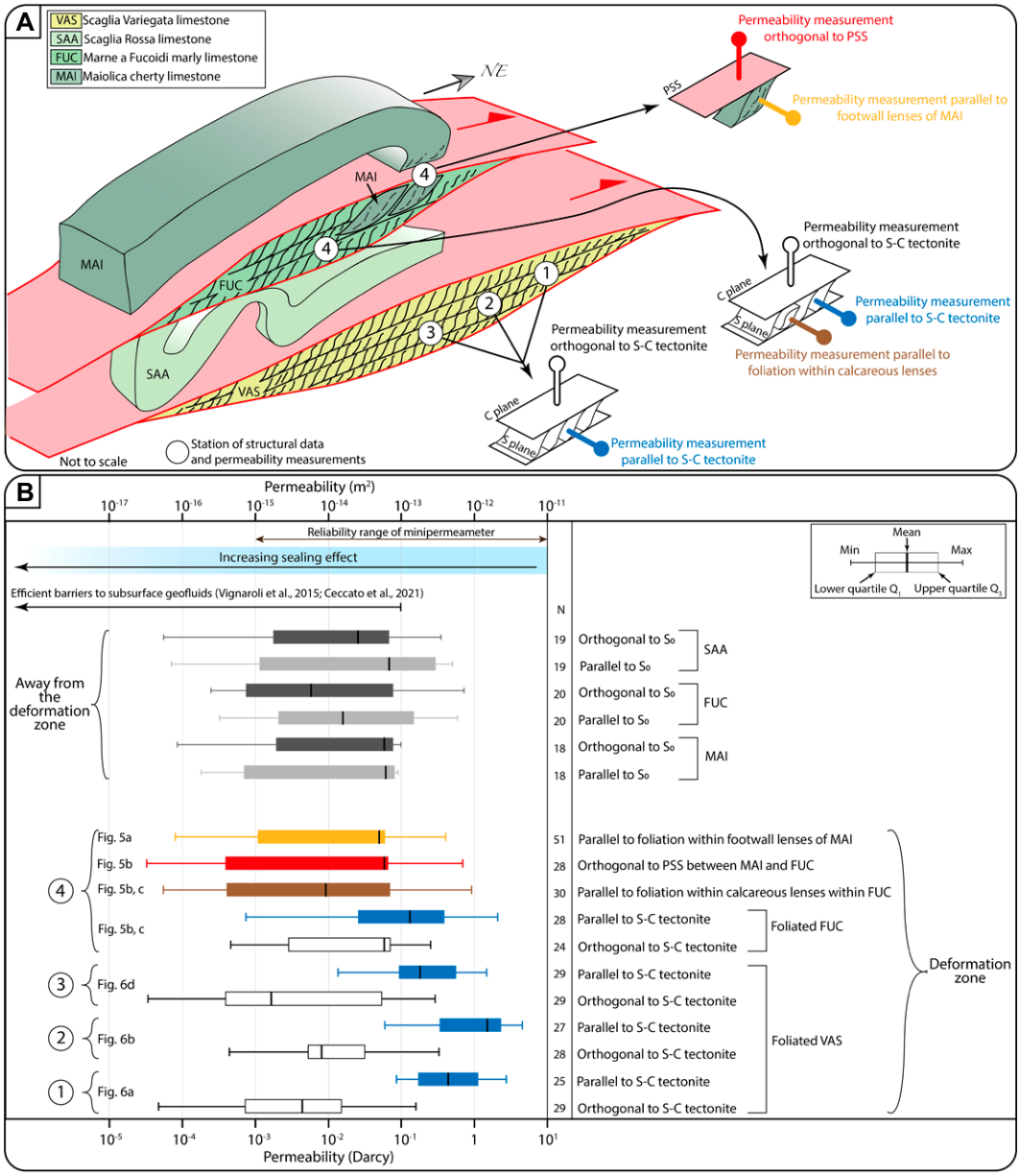

Figure 9. (A) 3-D schematic section of the key portion of the deformation zone showing the stations of structural data and permeability measurements. The orientation of permeability measurements with respect to the S-C/C' tectonites, principal slip surface (PSS), and calcareous lenses is also shown. (B) In situ air permeability data from the lithotypes involved into the deformation zone. Permeability measurements were collected (1) away from the deformation zone and (2) within the deformation zone (see Figs. 2C and 3 for the location of stations of permeability measurement).

1 M authigenic/syn-kinematic illite formed during brittle faulting (low temperature conditions) and of the $2M_1$ detrital illite (high temperature conditions), we normalized to 100% the proportion of $2M_1$ and 1 M illite (as determined by XRD analysis; histograms of Fig. 10A) plotting the data as apparent K-Ar age versus percentage of detrital illite, and linearly extrapolated to 0 and 100% $2M_1$ illite by ordinary least square regression (Fig. 10C). Although more sophisticated regression methods can be adopted to account for the uncertainties on the individual data points (e.g., York et al., 2004), these assume a Gaussian distribution of the uncertainty envelopes in both x and y coordinates, which are likely not valid for the quantified X-ray diffraction mineralogy proportions. By means of the adopted ordinary least square regression, the obtained IAA ages show that the age close to the last slip event recorded by GI11 is 6.9 ± 6.4 Ma and by GI12 is 6.2 ± 9.5 Ma (Fig. 10C). The age of the regressed detrital 2M1 illite recorded by sample GI11 is 162.8 ± 3 Ma and by sample GI12 is 158.1 ± 4.2 Ma (Fig. 10C).

5. DISCUSSION

5.1. Deformation Mechanisms

Orogenic compression in the study area has been shown to be strongly conditioned by the rheological contrasts associated with (1) Jurassic paleogeographic inheritances such as horsts and grabens and (2) lithological heterogeneities within the deformed clay-rich multilayer carbonate succession (e.g., Pierantoni et al., 2013; Cipriani, 2016, 2019; Santantonio et al., 2016; Curzi et al., 2020a). In the following, we elaborate on the mechanical role potentially played by lithological/stratigraphic features on strain partitioning within complex deformation zones, indeed the case of the STF.

5.1.1. Competence Contrast

The box anticline in the hanging wall of the main roof thrust (Figs. 4A and 4B) reflects the attitude of bedding of the (Jurassic) Mt. Sibilla–Mt. Priora PCP and its onlapping and overlying

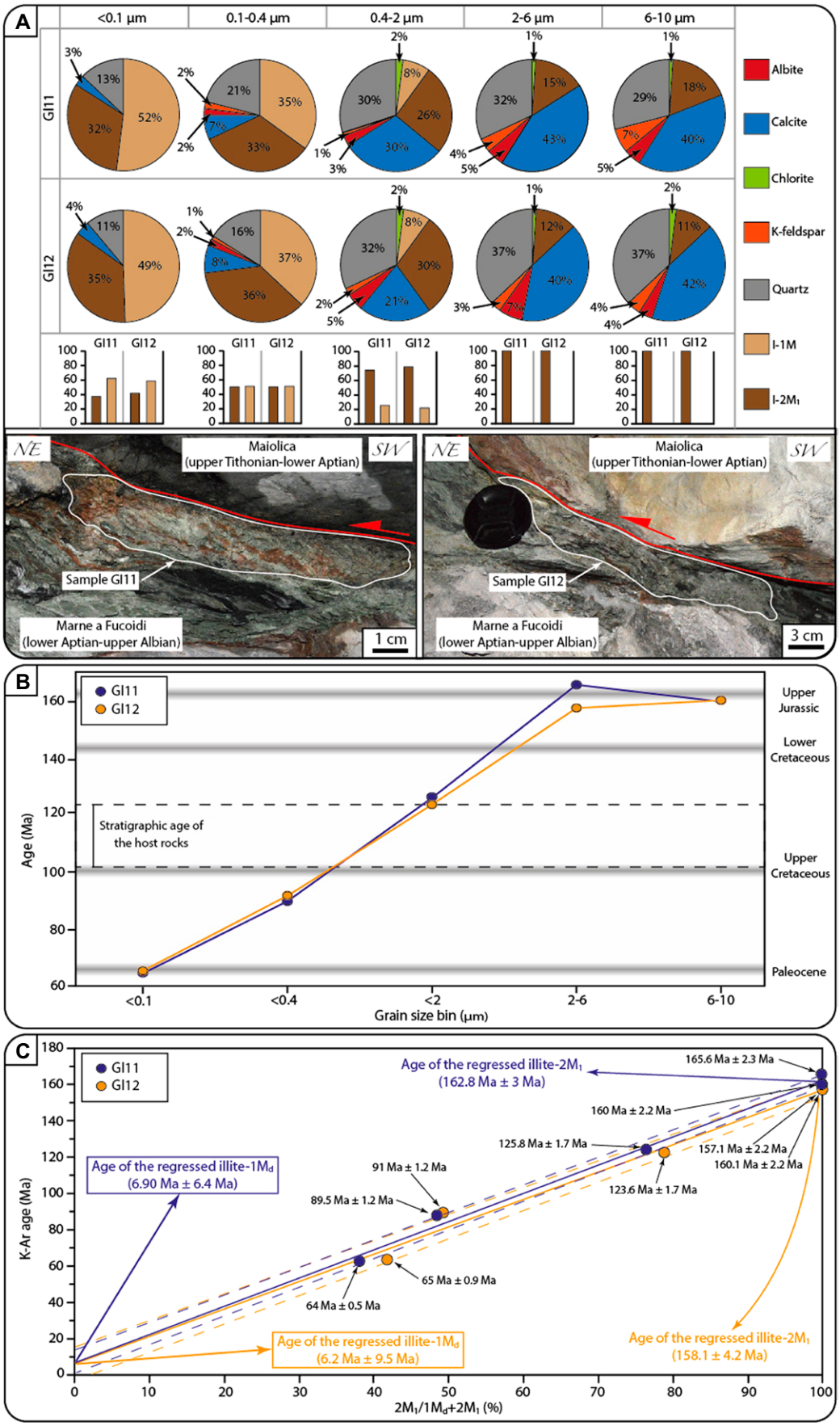

Figure 10. (A) X-ray semiquantitative analysis of clay gouges for samples GI11 and GI12. Bar diagrams show the percentage of illite polytypes normalized to 100 for each gran size fraction. Note the progressive increase of authigenic illite-1 M toward the finer fractions. The sampling sites of the dated fault gouge (samples GI11 and GI12) are shown. Both the samples were collected within the deformation zone, along the thrust that juxtaposes the Maiolica cherty limestones onto the Marne a Fucoidi marly limestones. (B) K-Ar age versus grain size. Dark gray horizontal bars define geological time intervals. The depositional age of the host rocks is shown. (C) Least square regression (continuous lines) and error envelop (dotted lines) of illite age analysis (IAA) for the clay gouges for samples GI11 and GI12. To estimate the ages of the authigenic illite-1 M end-member, which corresponds to the last faulting event recorded by the illite, K-Ar ages versus percentage of illite-2M1 (normalized to 100%) are plotted and linearly extrapolated to 0% illite-2M1. The age of the regressed detrital illite-2M1 and authigenic/synkinematic illite-1 M recorded by samples GI11 and GI12 are shown.

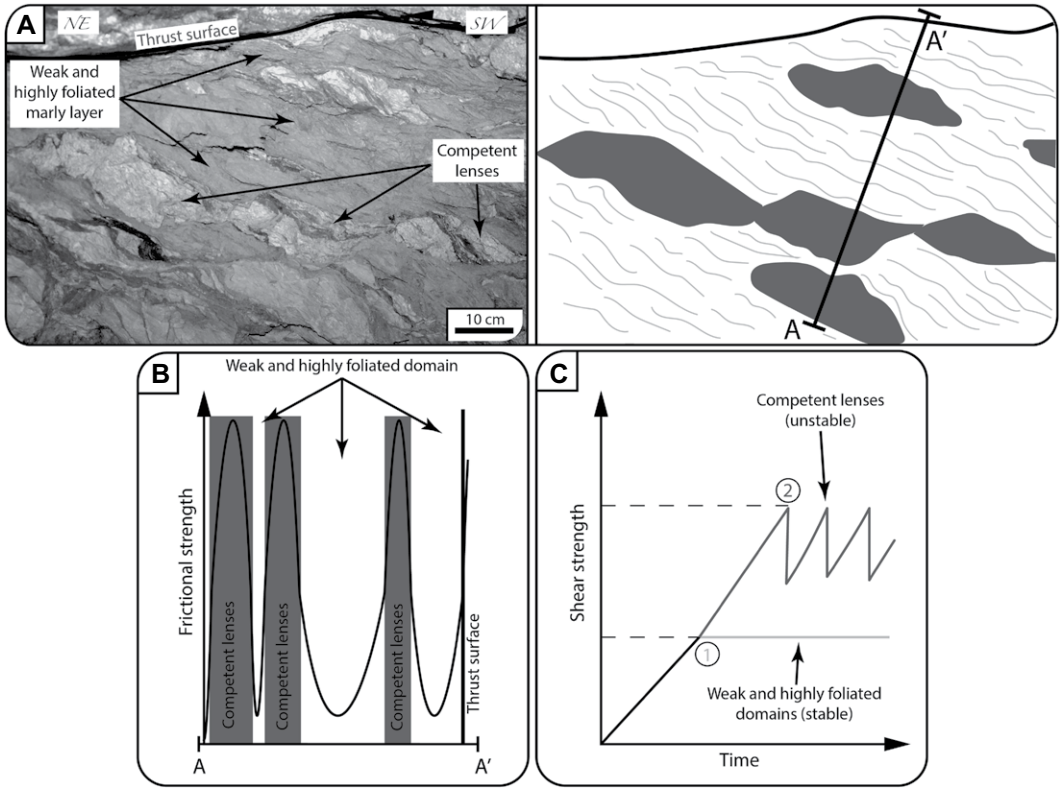

Figure 11. (A) Photograph and relative schematic drawing of competent calcareous lenses embedded within the highly foliated marly domain of the Marne a Fucoidi exposed below the thrust surface which juxtaposes the Maiolica limestones onto the Marne a Fucoidi marly limestones. (B) Curve showing frictional strength variation within weak highly foliated marly domains and competent lenses along the transect A–A′ through the schematic drawing in A. (C) Shear strength for a heterogeneous deformation zone. Weak and highly foliated marly domains are characterized by low frictional strength and exhibit stable (velocity-strengthening) frictional behavior. Competent lenses possess high frictional strength and exhibit potentially unstable and (velocity-weakening) frictional behavior.

pelagic deposits (Figs. 4A and 4B). However, the same structure was previously interpreted as the result of thrusting along a blind thrust (Cooper and Burbi, 1986; Calamita, 1990; Pierantoni et al., 2013; Pace et al., 2022a). The decametric overturned syncline within the structurally highest horse, which folds the Jurassic-lowermost Cretaceous pelagic sequence (to the west of the Calcare Massiccio block; Figs. 3, 4A, and 4B), is interpreted as the effect of buttressing of the Calcare Massiccio (considered to be a portion of the Mt. Sibilla-Mt. Priora Jurassic horst block in published maps in the area by Chiocchini et al., 1976; Cooper and Burbi, 1986; Pierantoni et al., 2013). Hence, plastic flow of the less competent pelagic rocks was locally hindered by the Calcare Massiccio, which acted as a rheologically more competent object.

5.1.2. Lithological and Structural Heterogeneities within the Multilayer Carbonate Succession

The pelagic succession within the ~300-m-thick deformation zone is represented by calcareous and marly rocks, which exhibit different styles of deformation. The relatively competent portions contain metric, poorly foliated sigmoidal lenses embedded within the weak and highly foliated marly domains and characterized by an imbricated internal structure (Fig. 5A). At the microscale, the relatively competent portions are characterized by poorly foliated cataclasite containing clasts of veined limestone and chert (Fig. 7), which formed during repeated shearing accompanied by transient fluid overpressure pulses (e.g., Sibson, 2000; Curzi et al., 2020a). Evidence for shearing is also provided by discrete thrust surfaces decorated by fault gouge lenses mostly along the contact between rock domains with different competence (Fig. 5).

The relatively less competent domains are also characterized by evidence of shearing as shown by pervasive S-C/C' fabrics (interpreted as the result of dominant simple-shear along the STF; e.g., Calamita et al., 2012; Pace et al., 2015, 2022b) associated with calcite veins along the S planes (i.e., orthogonal to the maximum stress orientation; Fig. 8D). These features demonstrate that the foliation planes acted as relatively weak surfaces along which dilation localized triggered by fluid overpressure (e.g., Bruna et al., 2019; Curzi et al., 2020a). Local and minor variations of the stress field, however, may have also contributed to the opening of veins parallel to the S planes during fluid overpressuring. Shearing is documented by (1) the presence of sharp shear planes (attesting to simple shear) bounding the calcite veins (Fig. 8D), (2) en-échelon calcite veins between sharp shear planes (Fig. 8D), and (3) boudinaged calcite veins (Fig. 8D). Boudinaged veins and calcareous blocks (Figs. 8C and 8D) also suggest a rotation of the relatively competent objects embedded within more marly domains during compression.

As discussed above, the ~300-m-thick STF deformation zone contains S-C/C' tectonites (Figs. 5, 6A, 6B, and 11A) and discrete cataclastic domains, discrete thrusts and competent lithons as well as discrete lenses (Figs. 5, 6A, 6B, and 11A). Coexisting distributed and localized deformation reflects the rheological contrast typical of carbonate multilayer successions (e.g., Tesei et al., 2013; Curzi et al., 2020a; Zuccari et al., 2022). Indeed, foliated domains are mostly found within the marly lithotypes, whereas sigmoidal lithons and cataclastic domains within the more competent carbonate lithotypes. Localized, discrete structures suggest high frictional strength and, potentially, an unstable frictional (seismic) behavior (Figs. 11B and 11C; Faulkner et al., 2003; Collettini et al., 2011; Tesei et al., 2014; Curzi et al., 2020a). On the other hand, fault rocks that attest to semi-brittle shearing and contain pervasive planar fabrics (S-C tectonites) are characterized by low frictional strength and are generally considered as resulting from aseismic deformation (Figs. 11B and 11C; Faulkner and Rutter, 2001; Faulkner et al., 2003; Collettini et al., 2011; Tesei et al., 2014; Curzi et al., 2020a).

Also, softening processes may be related to the development of S-C/C' fabrics during shearing of fine-grained marly lithotypes (e.g., Rutter, 1976; Tesei et al., 2014). Hardening, instead, is due to grain interlocking during cataclasis and to precipitation of calcite veins (within the S-C/C' tectonites), which can be stronger than the marly host rock (e.g., Kennedy and Logan, 1997; Tesei et al., 2014; Torgersen and Viola, 2014). Hence, in analogy with similar fault rocks and deformation zones, we propose that during compressional deformation, the frictional stress likely raised until it reached the frictional strength of the weak domains, and the deformation zone began to slip (Fig. 11C point 1). With continued shear, the tectonic stress likely increased and, when the shear stress reached the frictional strength of the competent domains (Fig. 11C point 2), frictional instability nucleated within the strong domains (e.g., Collettini et al., 2011). Such partitioning of deformation suggests that the mechanical evolution of the STF may have taken place by cyclically oscillating both in time (during the progressive compressional deformation) and space (within the ~300-m-thick deformation zone) between strain hardening and softening conditions (e.g., Hadizadeh, 1994; Tesei et al., 2014; Curzi et al., 2020a; Vignaroli et al., 2020). This mixed mechanical behavior suggests a sequence of compressional deformation events including (1) co-seismic rupturing characterized by high strain rate and frictional deformations and (2) inter-seismic creep under low strain rates by aseismic and low-to-non-frictional mechanisms (Fig. 11C; Faulkner and Rutter, 2001; Faulkner et al., 2003; Wibberley et al., 2008; Fagereng and Sibson, 2010; Collettini et al., 2011; Gratier et al., 2013; Tesei et al., 2014; Curzi et al., 2020a; Vignaroli et al., 2020). The switch between mechanisms typical of the co-seismic and inter-seismic stages may have been strongly influenced by pore pressure oscillations, as discussed below.

5.2. Implications on the Permeability Structure of Fault Zones

As a whole, clay-rich rocks are known to have relatively low permeability especially when they undergo compaction in response to tectonic and sedimentary load, and burial (e.g., King Hubbert and Rubey, 1959; Suppe, 2014; Giorgetti et al., 2016). The intrinsically low permeability of clay-rich rocks is also testified by the permeability measured out of the deformation zone, indicating that these lithotypes represent efficient hydraulic barriers, especially to fluid flow orthogonal to bedding (with permeability values up to $\sim 6 \times 10^{-5}$; Fig. 9B).

However, it has also been shown that (1) foliated fault rocks from experimental deformation and (2) fault gouge similar to those exposed in the study area represent efficient permeability barriers (with values from 10^{-4} to 10^{-10} D) to cross-foliation fluid flow, thus promoting overall sealing effects (Caine et al., 1996; Ikari et al., 2009; Faulkner et al., 2010; Mittempergher et al., 2011; Kawano et al., 2011; Gratier et al., 2013; Torgersen and Viola, 2014; Scuderi and Collettini, 2018). This is also corroborated by our permeability measurements from within the deformation zone (Figs. 9A and 9B). Indeed, the very low permeability orthogonal to the S-C tectonites and the PSS (up to ~3x 10^{-5} D; Fig. 9B) would confirm that such structural elements form hydraulic barriers to any across-fluid flow, which, in the case of gently to moderately dipping deformation zones, means along the sub-vertical dimension. Thus, because of the presence of (1) pervasive S-C/C' fabrics (Figs. 5B, 5C, 6A, and 6B), (2) closely spaced and amalgamated S planes forming up to ~1 cm thick bands of insoluble material (Figs. 8A, 8C, and 8D), which may account for a significant decrease of porosity and permeability (Angevine and Turcotte, 1983; Wu et al., 2023), (3) thrust surfaces also decorated by fault gouge (Figs. 5A and 10A), and (4) the aforementioned low permeability values within the STF deformation zone (Fig. 9B), the clay-rich multilayer carbonate succession within the deformation zone became an even lower permeability barrier during deformation, virtually preventing any significant fluid flow across the deformed rock volume (Faulkner et al., 2010; Kawano et al., 2011; Gratier et al., 2013; Farrell et al., 2014; Vannucchi, 2019; Wenning et al., 2021).

The relatively high values of permeability parallel to the S-C tectonites (Fig. 9B) are likely associated with microcracks developed along closely spaced pressure solution planes during exhumation and decompression. Our permeability data likely overestimate real permeabilities by a factor of ~1.7 (e.g., Fossen et al., 2011; Ceccato et al., 2021). Hence, (1) our data are used to understand the magnitude order of permeability differences between different tectonic structures within the deformation zones and (2) it is reasonable to assume that analogous buried structures could be characterized by even lower permeability values. Vignaroli et al. (2015) and Ceccato et al. (2021) interpret the $<\sim 10^{-1}$ D of measured permeabilities as pertaining to efficient barriers to subsurface geofluids (Fig. 9B). The same range of permeability to air belong to the thrust zone and host rocks (Fig. 9B), thus reinforcing the aforementioned sealing capacity of (1) low permeability marl and marly limestones and (2) tectonic structures.

It should be remembered that our permeability measurements mostly gage the primary porosity of the rock (i.e., only interstitial pores and no fractures/joints), particularly in the case of rocks not affected by the deformation zone. It is known, however, that thrust-related anticlines and synclines are diffusely jointed (e.g., Tavani et al., 2015), whereas joints are often healed, closed, and/or overprinted by pressure solution and shear processes in the thrust-related shear zones as shown for the case study in here (Figs. 7 and 8). Hence, we believe that the fluid barrier in our study case is mainly composed of the thrust-related deformation zone, as the host rocks in the footwall and hanging wall are affected by secondary permeability that did not contribute to the measured permeability (Fig. 9B). This concept is significantly reinforced by the fact that the STF is known, at the regional scale, as a hydrogeological aquiclude, whereas its hanging wall block is a fractured carbonate aquifer feeding important springs (Nanni and Vivalda, 2005; Mastrorillo and Petitta, 2014; Viaroli et al., 2021).

Recent studies from the Apennines based on meso/microstructural and geochemical results on similar deformation zones, fault rocks, and mineralizations have also documented that thrust-related deformation zones (especially in marl-rich successions) dominated by S-C fabrics and distributed deformation represent low-permeability barriers (Curzi et al., 2020a, 2021; Smeraglia et al., 2020). In the broader study area as well as in the central-northern Apennines, thrust-related structures like those described here are commonly reported and extensively documented (Coli and Sani, 1990; Calamita et al., 1991, 2012; Vannucchi et al., 2003; Tesei et al., 2014; Lena et al., 2015; Pace et al., 2015, 2022b; Curzi et al., 2020a, 2021; Satolli et al., 2020). Such structures are described as exhumed from 3 to 4 km depth, as demonstrated by the analysis of clay mineral assemblage, vitrinite reflectance, and low-temperature thermochronology studies (Aldega et al., 2007; Corrado et al., 2010; Fellin et al., 2022). On this ground, the STF deformation zone can be considered as an exposed analogue of buried thrust-related deformation zones affecting similar lithotypes. As such, it may have hindered the upward flow of deep fluids. In detail, as documented by recently published seismic reflection profiles across the central-northern Apennines, thrust-related deformed pelagic sequences can be identified down to ~6 km below the surface (Barchi et al., 2021). Hence, we suggest that buried thrust-related deformation zones within fold and thrust belts may act as barriers to the upward flow of fluids and thus compartmentalize the crust in distinct potential reservoirs, that would be juxtaposed along the moderately dipping thrust zones.

5.3. Seismotectonic Implications

In the occasion of the 2016 Amatrice-Norcia earthquakes, seismological evidence has highlighted that the SFT represented a permeability barrier at depth (between ~3 and 6 km), which would have steered fluid accumulation and overpressure below the thrust zone, particularly during pre-seismic stages (Improta et al., 2019; Gabrielli et al., 2022). This supports (1) our extrapolations from the surface to depth as to the low permeability of buried thrust zones and (2) the role of such hydraulic barriers in fluid accumulation, ponding, and overpressuring. On this ground, the STF may play an important role also in the current extensional seismicity pattern due to its regional extent and its inferred role of barrier to fluids (Gabrielli et al., 2022). In other words, Sibson's fault valve behavior (Sibson, 1981, 1992) may occur in the central Apennines, where the low-angle thrust zones and related stratigraphic imbricates act as top seals of pressurized fluid pockets, which may occasionally burst and escape upward through seismic valves represented by the conduits offered by active high-angle and thoroughgoing normal faults. We expand on this below, with reference to the 2016–2017 extensional seismic sequence.

Indeed, an intense debate is presently ongoing in the scientific community as to the role played by inherited thrusts in the extensional seismic sequences that recently affected the central Apennines. Such debate reflects into a plethora of quite different conceptual seismotectonic models, which contemplate positive and negative tectonic inversions (e.g., Pizzi and Galadini, 2009; Calamita et al., 2012; Scisciani et al., 2014, 2019; Pizzi et al., 2017; Tavarnelli et al., 2019), reactivation of the early thrusts as transfer faults or extensional décollements in the present tectonic regime (Pizzi et al., 2017; Improta et al., 2019; Michele et al., 2020), or simply seismic normal faults cutting pre-existing fossil thrusts (e.g., Porreca et al., 2018; Mancinelli et al., 2019). The influence of lithological control on fluid pressure build-up and drop within the belt is also being considered as a potential factor steering the overall seismotectonic style of the central Apennines (Trippetta et al., 2010; Mancinelli et al., 2019; Carminati et al., 2020). The debate has been further animated by recent models whereby earthquakes (main- and aftershocks) associated with the 2016–2017 Amatrice-Norcia seismic sequence (nucleated along the Mt. Gorzano normal fault and the adjacent Mt. Vettore fault system; Lavecchia et al., 2016; Chiaraluce et al., 2017; Fig. 12A) are proposed to have mostly localized in the immediate footwall of regional thrust planes (Buttinelli et al., 2021; Fig. 12B) and/or within thrust sheets dissected by normal faults (Barchi et al., 2021; Fig. 12B). These contrasting ideas stem from different interpretations of quite low-resolution seismic reflection profiles and are mainly related to the potential involvement of the pre-Triassic basement during thrusting and different crosscutting relationships and displacement between orogenic and post-orogenic structures (Fig. 12B). Regardless of these interpretations, it has been shown that the 2016–2017 seismic sequence was preempted by fluid accumulation, ponding, and overpressuring within the pile of thrust sheets (De Luca et al., 2018; Chiarabba et al., 2020) and accompanied by slight changes of the geochemical signature of groundwaters from some springs in the central Apennines (Barberio et al., 2017; Barbieri et al., 2020). The sequence was then accompanied and followed by a large outflow of groundwater and CO_2 at the Earth's surface (Petitta et al., 2018; Chiodini et al., 2020; Mastrorillo et al., 2020). Taken altogether, this evidence for the 2016–2017 seismic sequence suggests that fluid overpressure at depth may have played a major role in triggering the seismic swarm (see also Chiarabba et al., 2020; Convertito et al., 2020; Malagnini et al., 2022). In particular, fluids possibly accumulated at depth for a few months (according to the data produced by Barberio et al., 2017; De Luca et al., 2018; Martinelli et al., 2020) before the onset of the extensional sequence. Indeed, Chiarabba et al. (2020) documented a large Vp/Vs anomaly in the lowest part of the Apennines thrust wedge possibly connected with pre-seismic fluid accumulation. This may be associated with the sealing effect of lithological contacts (Trippetta et al., 2010; Barchi et al., 2021) or of the widespread Triassic evaporites at the base of many thrust sheets of the central Apennines (Trippetta et al., 2010; Fig. 13A). It is also reasonable that buried marly lithotypes also inhibited upward fluid flow (Suppe, 2014). In addition to these lithological effects, we suppose that a buried analogue of the exposed STF deformation zone may have represented an effective hydraulic barrier not only during orogenic compressional deformation, but also during the post-compressional extensional tectonics in the area. This hypothesis is corroborated by the structural and permeability results discussed above. The sealing effect of the deformation zone may have even been further enhanced by the presence of evaporite layers in the thrust sheets (Figs. 13A and 13B). Hence, we hypothesize that, before the 2016–2017 seismic sequence, such a low-permeability barrier may have possibly caused fluid overpressuring in the footwall of the thrust zone, thus eventually triggering the earthquake sequence (Fig. 13A). Some deep fluids likely leaked upward across the thrust-related barrier by locally exploiting the higher permeability provided by rock volumes characterized by dilatant brittle deformation features associated with the younger normal faults, as demonstrated by pre-seismic deep CO_2 and anomalous elements detected in some springs of the central Apennines (Barberio et al., 2017; Boschetti et al., 2019; Barbieri et al., 2020; Martinelli et al., 2020; Fig. 13A) and microseismicity localized within the stacked thrust sheets (Fig. 13). The onset of the seismic sequence may itself have caused the partial disruption of the hydraulic barrier represented by the thrust sheets, as demonstrated by the syn- and post-seismic massive discharge of groundwater in central Apennines (Petitta et al., 2018; Chiodini et al., 2020; Mastrorillo et al., 2020; Fig. 13B), also observed during the 2009 L'Aquila seismic sequence (Chiarabba et al., 2022). Earthquakes likely increased the structural permeability by fracturing thus allowing the upward flow of overpressured CO_2-rich fluids. We thus envisage a model of pre-seismic accumulation and overpressuring of fluids in the lower portions of the thrust wedge mostly determined by the imbricated and duplicated architecture of the wedge itself coupled with lithological contrasts, followed by a syn- and post-seismic upward flow and surficial discharge of at least part of these fluids (Figs. 13A and 13B).

After the earthquakes, due to the coseismic pressure drop and depressurization connected with the upward flow, fluids may have precipitated carbonate minerals within the open fractures, thus sealing again the rock volumes (Sibson, 1990). We believe, therefore, that fracture permeability is likely transient and cyclically oscillates during the extensional seismic cycles as influenced by the evolving fracturing along the active normal faults and by steady barrier to fluids constituted by thrust zones. The proposed process is consistent with the fault-valve behavior (e.g., Sibson, 1981, 1990; Viola et al., 2006) and with recent evidence from Curzi et al. (2021), who documented fluid circulation along the Mt. Gorzano fault connected with extensional faulting within an open fluid circuit, contrasting with the closed one connected with thrust faulting in the same study area. The fault valve behavior has already been proposed for earthquakes and seismicity in Italy (e.g., Chiarabba et al., 2022) and worldwide (e.g., Nevada, USA: Jansen et al., 2019; Mexico: Williams et al., 2017; and Japan: Sibson, 2007), and we also believe that, if the studied thrust zone presently exerts its influence on the seismotectonic activity of normal faults by modulating the fluid pressure, the same idea must have been valid also for the preceding activity of the thrust itself. As discussed above, meso- and microstructural evidence suggests that inter- and co-seismic deformations were

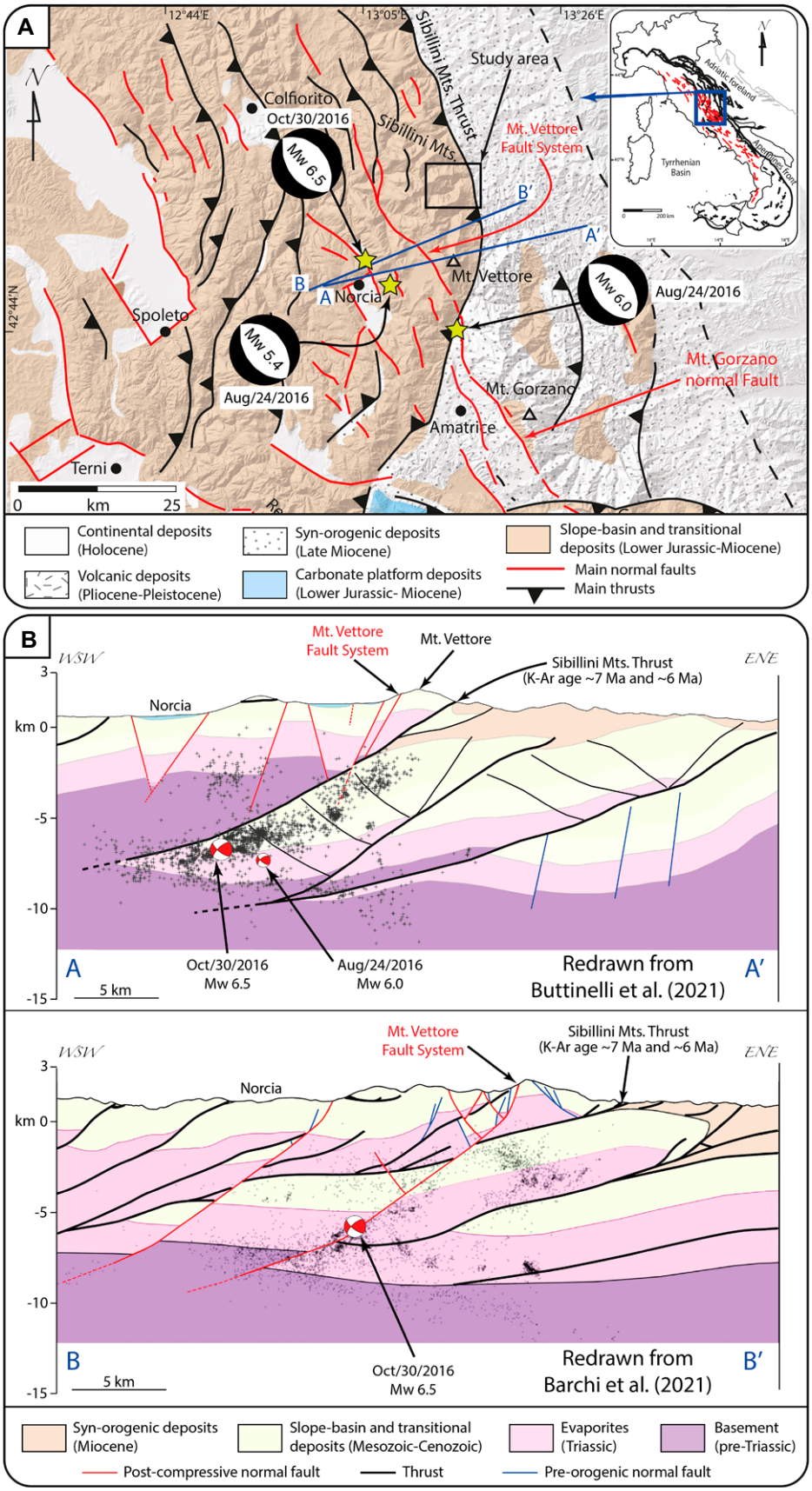

modulated by pore pressures influenced, in turn, by the sealing effect of the thrust itself.

5.4. K-Ar Constraints and Tectonic Implications

In the Sibillini Mts., indirect time constraints on compressional deformation can be derived from the age of youngest syn-orogenic deposits (Laga formation, Messinian *p.p*) exposed ~3–4 km to the east of the study area (in the footwall of the STF; Pierantoni et al., 2013; Figs. 2C and 2D). Based on the age of these deposits, an overall Messinian-late Pliocene age (between ca. 7 Ma and ca. 3 Ma) has previously been suggested for the compressional tectonics in this area (Calamita and Deiana, 1988; Calamita, 1990; Calamita et al., 2012; Fig. 14). Our K-Ar ages represent, therefore, the first absolute time constraints on compression accommodated along the most external exposed thrust of the central-northern Apennine belt (Fig. 14).

The obtained grain size-age correlation for samples GI11 and GI12 (Fig. 10B) is interpreted as resulting from the mixing between detrital illite-2M$_1$ inherited from the host rock (lowermost Aptian-upper Albian) and syn-kinematic illite-1 M formed during the last recorded increment of faulting (e.g., Pevear, 1999; Viola et al., 2018). Also, the K-Ar age of the finest fraction is considered to be the closest to the age of the last recorded faulting episode (Torgersen et al., 2015; Curzi et al., 2020a, 2020b; Tartaglia et al.,

Figure 12. (A) Simplified structural map of the central Apennines showing the main focal mechanisms and mainshocks from the 2016–2017 Amatrice-Norcia seismic sequence. (B) Geological cross section across the Sibillini Thrust Front (STF) and the Mt. Vettore normal fault systems. The sections A–A′ and B–B′ are redrawn and modified from Buttinelli et al. (2021) and Barchi et al. (2021), respectively. Although the interpretation of the subsurface geometries is different between the two geological cross sections, note that the hypocenters of the 2016–2017 Amatrice-Norcia seismic sequence are essentially localized below the thrust systems. The 2016–2017 Amatrice-Norcia seismic sequence and the focal mechanisms of the mainshocks (from http://terremoti.ingv.it/catalog and Scognamiglio et al., 2018 and Barchi et al., 2021) are projected along the geological cross section. The K-Ar ages of the Sibillini Mts. Thrust are also shown. The trace of the cross sections is shown in A.

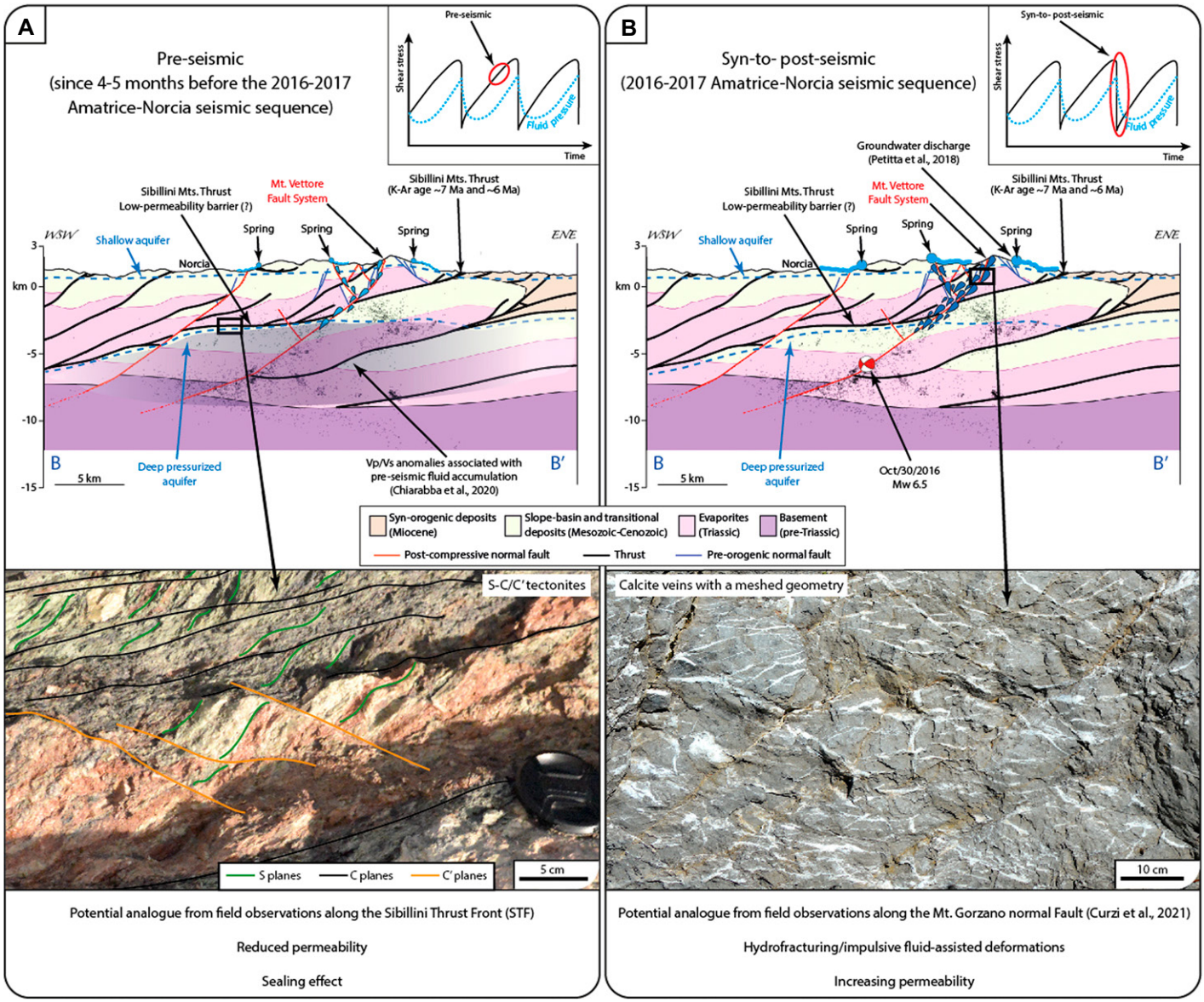

Figure 13. Conceptual model for fluid-assisted extensional deformation associated with the 2016–2017 Amatrice-Norcia seismic sequence. (A) During the pre-seismic phase (starting 4–5 months before the seismic sequence), evaporite-made or bounded thrust sheets and buried compressional (orogenic) deformation zones acted as hydraulic barriers to the flow of deep pressurized fluids, as testified by Vp/Vs anomalies at 5–10 km depth. Only some deep fluids leaked upward and gave rise to pre-seismic deep CO_2 and anomalous elements in some springs of the central Apennines. A representative potential analogue of fault rocks with sealing effect within deep thrust-related deformation zone is shown and arise from field observations along the Sibillini Thrust Front. (B) The pressurized fluids beneath the thrust zones and sheets probably triggered seismic extensional faulting so that the hydraulic barriers became disrupted and permitted rapid and abundant upward flow of fluids and associated groundwater discharge during the syn-/post-seismic phase. A representative potential analogue of structures associated with pulsed syn-/post-seismic upward flow of fluids is shown. This model is a synthesis of field evidence from this study, hydrogeochemical evidence from Barberio et al. (2017), Petitta et al. (2018), Boschetti et al. (2019), Barbieri et al. (2020), Chiodini et al. (2020), Martinelli et al. (2020), and Mastrorillo et al. (2020), geophysical evidence from Chiarabba et al. (2020) and Convertito et al. (2020), structural and geochemical evidence from Curzi et al. (2021), and seismic evidence from Barchi et al. (2021) and Buttinelli et al. (2021). The cross section and the instrumental seismicity from the 2016–2017 Amatrice-Norcia seismic sequence are from Barchi et al. (2021). The trace of the cross section is shown in Figure 12A.

2020). The last recorded event, however, does not necessarily coincide with the last tectonic movement along the thrust surface or within its deformation zone. Additionally, the date of the finest fraction might still represent a mixed age, partially reflecting the isotopic contribution of small amounts of K-bearing minerals reworked from the host rock into the fault gouge during cataclasis (Clauer, 2013).

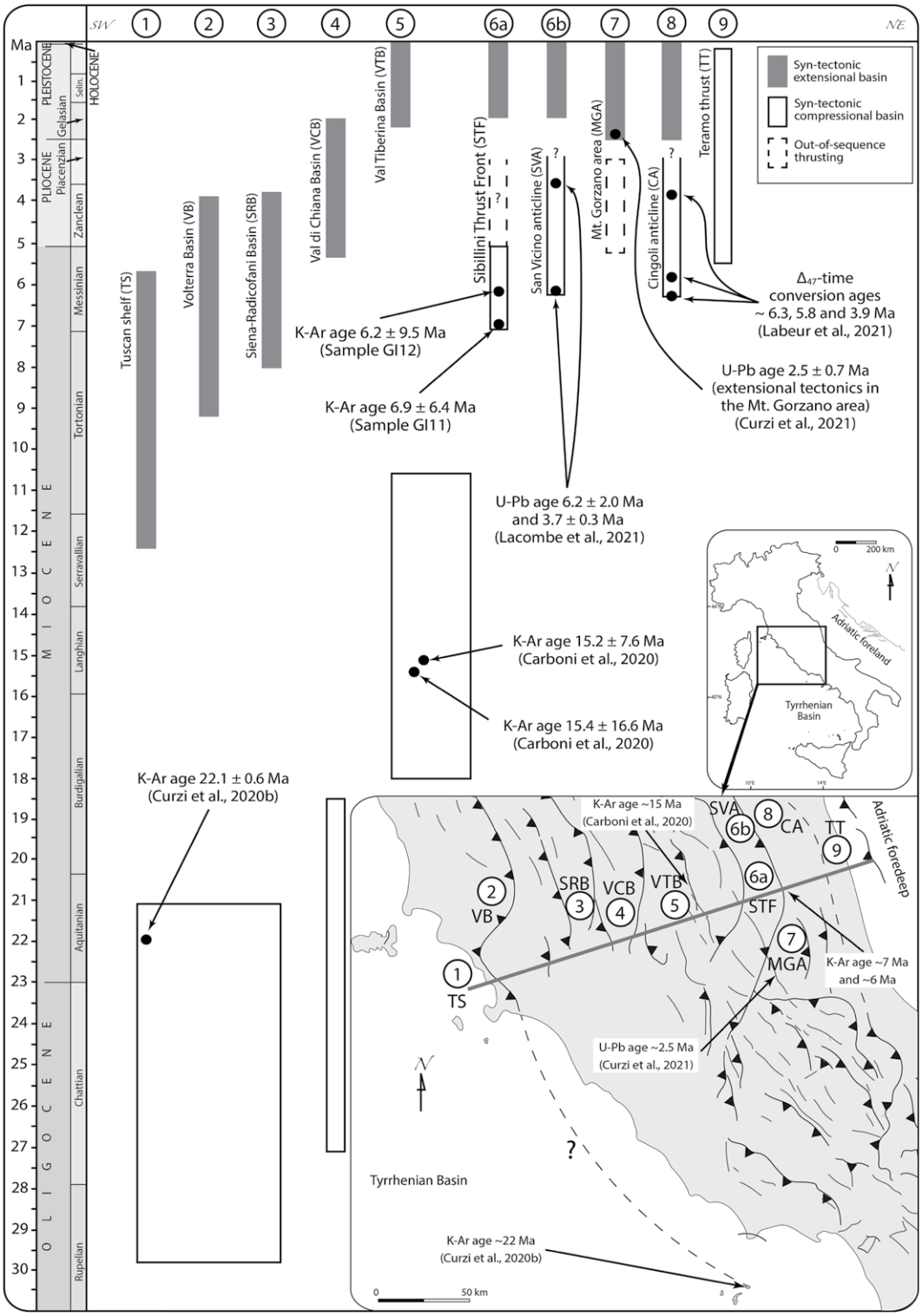

Figure 14. Time-distance diagram, including syn-tectonic extensional and compressional basins and periods of extensional and compressional phases in the central-northern Apennines (data from Barchi, 2010; Bigi et al., 2011; Carboni et al., 2020; Curzi et al., 2020b, 2021; Labeur et al., 2021; Lacombe et al., 2021). Notice that K-Ar ages are consistent with the proposed temporal evolution of the easternmost northern Apennine system.

To reduce the effects of contamination of illite-2M_1 inherited from the host rock and, therefore, to derive geologically meaningful radiometric ages, the Illite Age Analysis (IAA) approach (Pevear, 1999) was adopted (Fig. 10C). However, when dealing with K-Ar dating of syn-kinematic clay minerals in fault gouge formed at the expense of rocks rich of terrigenous components, the mixing between inherited and newly formed syn-kinematic K-bearing minerals cannot always be completely deconvoluted by the IAA approach (Pevear, 1999; Carboni et al., 2020; Curzi et al., 2020a). Hence, in light of the large errors associated with the regressed K-Ar IAA ages, only a tentative interpretation is possible. These uncertainties notwithstanding, recent studies from the Apennines that applied K-Ar dating to gouges formed at the expense of terrigenous rocks have demonstrated the general reliability of the IAA approach despite the large errors

associated with data regression (Carboni et al., 2020; Curzi et al., 2020a).

In our study, it is important to stress that the calculated K-Ar IAA ages (Fig. 10C) are consistent with: (1) other independent biostratigraphic and stratigraphic time constraints available for the STF (between ca. 7 Ma and ca. 3 Ma; Calamita and Deiana, 1988; Calamita et al., 1990, 2012; Pierantoni et al., 2013; Fig. 14); (2) U-Pb radiometric ages on syn-tectonic carbonates associated with the San Vicino anticline, which represents the northern prosecution of the STF (and located ~30 km to the north of the study area. These radiometric constraints indicate the beginning of compressional deformation in the area at ca. 6 Ma (Lacombe et al., 2021; Fig. 14); and (3) time constraints derived from the Cingoli anticline (located ~30 km to the northeast of the STF), which were estimated through clumped isotope thermometry-time conversion and which indicate an age of ca. 6 Ma for the onset of compressional deformation (Labeur et al., 2021; Fig. 14). Hence, based on our IAA results, the illite-1 M can be interpreted as having formed during slip along the thrust. It should also be pointed out that samples GI11 and GI12 were both collected along the same thrust surface (i.e., at the tectonic contact between Maiolica and Marne a Fucoidi; Figs. 5A and 10A). For this reason, the K-Ar IAA ages from distinct samples mutually validate and, additionally, constrain slip to the same thermo-tectonic event, which spans the 6.9–6.2 Ma (early-middle Messinian) time interval.

6. CONCLUSIONS

This study stresses the role of inherited structures (specifically, the role of older inactive thrust zones in a seismically active extensional domain) on fluid circulation and overpressuring and consequent earthquakes triggering. In the Apennines we show that imbricated thrusts and thrust-related deformation zones as old as ca. 7 Ma (Messinian) provide effective barriers to uprising fluid circulation. Consequent fluid accumulation below the low-permeability thrust zone increases fluid pressure and eventually may control active post-orogenic extensional faulting, triggering seismic slip along normal faults prone to slip. The importance of the structural inheritance is even more accentuated if we also consider the fact that the hydraulic properties of the thrust zones are determined or influenced by the type of deformation (e.g., foliation, plastic deformation), which is in turn ruled by rheological contrasts and/or paleogeographic domains capable of counteracting the tectonic shortening (buttressing effect). These inferences are mostly drawn on the assumption, which should be further corroborated, that the exposed STF is a credible and reliable analogue of buried thrust zones in the central Apennines.

Our work documents in detail the architecture and permeability structure of a complex thrust zone and allows us to draw the following conclusions:

(1) Rheological contrasts strongly influenced the development of the studied thrust-related deformation zone, which formed under a mixed rheological behavior (strain softening and strain hardening) during fluid-assisted deformation.

(2) Marl-rich host rocks are characterized by low permeability, which varies by up to one order of magnitude when measured parallel (mean values between $\sim 6 \times 10^{-2}$ and $\sim 2 \times 10^{-2}$ D) to orthogonal (mean values between $\sim 6 \times 10^{-2}$ and $\sim 7 \times 10^{-3}$ D) to bedding.

(3) The permeability becomes lower within the thrust zone, where the PSS (which has the lowest measured minimum value of $\sim 3 \times 10^{-5}$ D) and S-C tectonites (with permeability parallel to the S-C tectonites up to five orders of magnitude higher than that measured orthogonally to S-C tectonites) represent hydraulic barriers to sub-vertical fluid flow.

(4) Buried structures in the central Apennines, analogous to the studied thrust zone, may currently act at depth as hydraulic barriers to ascending fluids and thus contribute to fluid overpressure during the ongoing extensional tectonic activity. Fluid overpressure may have triggered and accompanied the 2016–2017 destructive seismic sequence in the central Apennines.

(5) Our model is consistent with the fault-valve model that can explain seismicity in the central Apennines as well as in other seismically active regions elsewhere. As the efficiency of Sibson's fault valve behavior is usually site-specific, the example provided in this paper adds further evidence to the database of known instances, thus providing a new reference to the scientific community.

ACKNOWLEDGMENTS

This work has been funded by Progetto di avvio alla ricerca 2019 (M. Curzi), Progetti di Ateneo Sapienza 2021 (E. Carminati). Clay mineral analysis was performed at the Academic Laboratory of Basin Analysis (ALBA) at Roma Tre University. R. Xie is thanked for assistance with K analysis. G. Innamorati is thanked for her kind support in the field. We thank D. Mannetta for preparation of thin sections. We thank the Parco Nazionale dei Monti Sibillini, and the Montefortino and Montemonaco municipalities for facilitating the logistics during the field work within the Gole dell'Infernaccio. We thank Gallo, Anastasia, and the whole family for their warm hospitality. The editor, the associate editor (E. Tavarnelli), P. Pace, and an anonymous reviewer are thanked for their comments and revisions. Analytical data are reported in the paper and in the supporting information. Part of the study was conducted in the framework of the FAST project (Fault Architecture in Space and Time; PI: G. Viola), a research project funded by the Italian Ministry for University and Research (MUR) with the PRIN 2020 funding action (CUP J33C22000170001).

REFERENCES CITED

Agosta, F., and Kirschner, D.L., 2003, Fluid conduits in carbonate-hosted seismogenic normal faults of central Italy: Journal of Geophysical Research: Solid Earth, v. 108, p. 1–13, https://doi.org/10.1029/2002JB002013.

Aldega, L., Botti, F., and Corrado, S., 2007, Clay mineral assemblages and vitrinite reflectance in the Laga Basin (Central Appenines, Italy): What do they record?: Clays and Clay Minerals, v. 55, p. 504–518, https://doi.org/10.1346/CCMN.2007.0550505.

Aldega, L., Viola, G., Casas-Sainz, A., Marcén, M., Román-Berdiel, T., and Van der Lelij, R., 2019, Unraveling multiple thermotectonic events accommodated by crustal-scale faults in northern Iberia, Spain: Insights from K-Ar dating of clay gouges: Tectonics, v. 38, p. 3629–3651, https://doi.org/10.1029/2019TC005585.

Angevine, C.L., and Turcotte, D.L., 1983, Porosity reduction by pressure solution: A theoretical model for quartz arenites: Geological Society of America Bulletin, v. 94, p. 1129–1134, https://doi.org/10.1130/0016-7606(1983)94<1129:PRBPSA>2.0.CO;2.

Barberio, M.D., Barbieri, M., Billi, A., Doglioni, C., and Petitta, M., 2017, Hydrogeochemical changes before and during the 2016 Amatrice-Norcia seismic sequence (central Italy): Scientific Reports, v. 7, p. 1–12, https://doi.org/10.1038/s41598-017-11990-8.

Barbieri, M., Boschetti, T., Barberio, M.D., Billi, A., Franchini, S., Iacumin, P., Selmo, E., and Petitta, M., 2020, Tracing deep fluid source contribution to groundwater in an active seismic area (central Italy): A combined geothermometric and isotopic ($\delta^{13}C$) perspective: Journal of Hydrology (Amsterdam), v. 582, https://doi.org/10.1016/j.jhydrol.2019.124495.

Barchi, M.R., 2010, The Neogene-Quaternary evolution of the Northern Apennines: Crustal structure, style of deformation and seismicity: Journal of the Virtual Explorer, v. 36, no. 10, https://doi.org/10.3809/jvirtex.2010.00220.

Barchi, M.R., Carboni, F., Michele, M., Ercoli, M., Giorgetti, C., Porreca, M., Azzaro, S., and Chiaraluce, L., 2021, The influence of subsurface geology on the distribution of earthquakes during the 2016–2017 Central Italy seismic sequence: Tectonophysics, v. 807, https://doi.org/10.1016/j.tecto.2021.228797.

Bigi, S., Casero, P., and Ciotoli, G., 2011, Seismic interpretation of the Laga Basin; constraints on the structural setting and kinematics of the Central Apennines: Journal of the Geological Society, v. 168, p. 179–190, https://doi.org/10.1144/0016-76492010-084.

Billi, A., and Tiberti, M.M., 2009, Possible causes of arc development in the Apennines, central Italy: Geological Society of America Bulletin, v. 121, p. 1409–1420, https://doi.org/10.1130/B26335.1.

Boncio, P., Lavecchia, G., Milana, G., and Rozzi, B., 2004, Seismogenesis in Central Apennines, Italy. An integrated analysis of minor earthquake sequences and structural data in the Amatrice-Campotosto area: Annals of Geophysics, v. 47.

Boschetti, T., Barbieri, M., Barberio, M.D., Billi, A., Franchini, S., and Petitta, M., 2019, CO_2 inflow and elements desorption prior to a seismic sequence, Amatrice-Norcia 2016, Italy: Geochemistry, Geophysics, Geosystems, v. 20, no. 5, p. 2303–2317, https://doi.org/10.1029/2018GC008117.

Bruna, P.O., Lavenu, A.P.C., Matonti, C., and Bertotti, G., 2019, Are stylolites fluid-flow efficient features?: Journal of Structural Geology, v. 125, p. 270–277, https://doi.org/10.1016/j.jsg.2018.05.018.

Butler, R.W.H., and Mazzoli, S., 2006, Styles of continental contraction: A review and introduction, *in* Mazzoli, S., and Butler, R.W.H., eds., Styles of Continental Contraction: Geological Society of America Special Paper 414, https://doi.org/10.1130/2006.2414(01).

Buttinelli, M., Petracchini, L., Maesano, F.E., D'Ambrogi, C., Scrocca, D., Marino, M., Capotorti, F., Bigi, S., Cavinato, G.P., Mariucci, M.T., Montone, P., and Di Bucci, D., 2021, The impact of structural complexity, fault segmentation, and reactivation on seismotectonics: Constraints from the upper crust of the 2016–2017 Central Italy seismic sequence area: Tectonophysics, v. 810, https://doi.org/10.1016/j.tecto.2021.228861.

Caine, J.S., Evans, J.P., and Forster, C.B., 1996, Fault zone architecture and permeability structure: Geology, v. 24, p. 1025–1028, https://doi.org/10.1130/0091-7613(1996)024<1025:FZAAPS>2.3.CO;2.

Calamita, F., 1990, Thrusts and fold-related structures in the Umbria-Marche Apennines (Central Italy): Annals of Tectonics, v. 4, p. 83–117.

Calamita, F., and Deiana, G., 1988, The arcuate shape of the Umbria-Marche-Sabina Apennines (central Italy): Tectonophysics, v. 146, p. 139–147, https://doi.org/10.1016/0040-1951(88)90087-X.

Calamita, F., Deiana, G., and Pizzi, A., 1990, Neogene evolution of an arcuate structure in the Umbria-Marche Apennines: Rivista Italiana di Paleontologia e Stratigrafia, v. 96, p. 297–308.

Calamita, F., Decandia, F.A., Deiana, G., and Fiori, A.P., 1991, Deformation of S-C tectonites in the Scaglia Cinera Formation in the Spoleto area (Southeast Umbria): Bollettino della Società Geologica Italiana, v. 110, p. 661–665.

Calamita, F., Satolli, S., and Turtù, A., 2012, Analysis of thrust shear zones in curve-shaped belts: Deformation mode and timing of the Olevano-Antrodoco-Sibillini thrust (Central/Northern Apennines of Italy): Journal of Structural Geology, v. 44, p. 179–187, https://doi.org/10.1016/j.jsg.2012.07.007.

Calamita, F., di Domenica, A., and Pace, P., 2018, Macro- and meso-scale structural criteria for identifying prethrusting normal faults within foreland fold-and-thrust belts: Insights from the Central-Northern Apennines (Italy): Terra Nova, v. 30, p. 50–62, https://doi.org/10.1111/ter.12307.

Carboni, F., Viola, G., Aldega, L., Van der Lelij, R., Brozzetti, F., and Barchi, M.R., 2020, K-Ar fault gouge dating of Neogene thrusting: The case of the siliciclastic deposits of the Trasimeno Tectonic Wedge (Northern Apennines, Italy): Italian Journal of Geosciences, v. 139, p. 300–308, https://doi.org/10.3301/IJG.2020.06.

Carminati, E., Lustrino, M., Cuffaro, M., and Doglioni, C., 2010, Tectonics, magmatism and geodynamics of Italy: What we know and what we imagine: Journal of the Virtual Explorer, v. 36, https://doi.org/10.3809/jvirtex.2010.00226.

Carminati, E., Lustrino, M., and Doglioni, C., 2012, Geodynamic evolution of the central and western Mediterranean: Tectonics vs. igneous petrology constraints: Tectonophysics, v. 579, p. 173–192, https://doi.org/10.1016/j.tecto.2012.01.026.

Carminati, E., Bignami, C., Doglioni, C., and Smeraglia, L., 2020, Lithological control on multiple surface ruptures during the 2016–2017 Amatrice-Norcia seismic sequence: Journal of Geodynamics, v. 134, https://doi.org/10.1016/j.jog.2019.101676.

Cavinato, G.P., and De Celles, P.G., 1999, Extensional basins in the tectonically bimodal central Apennines fold-and-thrust belt, Italy: Response to corner flow above a subducting slab in retrograde motion: Geology, v. 27, p. 955–958, https://doi.org/10.1130/0091-7613(1999)027<0955:EBITTB>2.3.CO;2.

Ceccato, A., Viola, G., Tartaglia, G., and Antonellini, M., 2021, In-situ quantification of mechanical and permeability properties on outcrop analogues of offshore fractured and weathered crystalline basement: Examples from the Rolvsnes granodiorite, Bømlo, Norway: Marine and Petroleum Geology, v. 124, https://doi.org/10.1016/j.marpetgeo.2020.104859.

Centamore, E., Chiocchini, M., Deiana, G., Micarelli, A., and Pieruccini, U., 1971, Contributo alla conoscenza del Giurassico dell'Appenino umbro-marchigiano: Studi Geologici Camerti, v. 1, p. 7–90.

Chiarabba, C., Amato, A., Anselmim, M., Baccheschi, P., Bianchi, I., Cattaneo, M., Cecere, G., Chiaraluce, L., Ciaccio, M.G., De Gori, P., De Luca, G., Di Bona, M., Di Stefano, R., Faenza, L., Govoni, A., Improta, L., Lucente, F.P., Marchetti, A., Margheriti, L., Mele, F., Michelini, A., Monachesi, G., Moretti, M., Pstori, M., Piana Agostinetti, N., Piccinini, D., Roselli, P., Seccia, D., and Valoroso, L., 2009, The 2009 L'Aquila (central Italy) Mw6.3 earthquake: Main shock and aftershocks: Geophysical Research Letters, v. 36, https://doi.org/10.1029/2009GL039627.

Chiarabba, C., De Gori, P., Segou, M., and Cattaneo, M., 2020, Seismic velocity precursors to the 2016 Mw 6.5 Norcia (Italy) earthquake: Geology, v. 48, p. 924–928, https://doi.org/10.1130/G47048.1.

Chiarabba, C., De Gori, P., Valoroso, L., Petitta, M., and Carminati, E., 2022, Large extensional earthquakes push-up terrific amount of fluids: Scientific Reports, v. 12, no. 14597, https://doi.org/10.1038/s41598-022-18688-6.

Chiaraluce, L., Di Stefano, R., Tinti, E., Scognamiglio, L., Michele, M., Casarotti, E., Cattaneo, M., De Gori, P., Chiarabba, C., Monachesi, G., Lombardi, A., Valoroso, L., Latorre, D., and Marzorati, S., 2017, The 2016 central Italy seismic sequence: A first look at the mainshocks, aftershocks, and source models: Seismological Research Letters, v. 88, p. 757–771, https://doi.org/10.1785/0220160221.

Chiocchini, M., Deiana, G., Micarelli, A., Moretti, A., and Pieruccini, U., 1976, Geologia dei Monti Sibillini nord-orientali: Studi Geologici Camerti, v. 2, p. 7–44.

Chiodini, G., Cardellini, C., di Luccio, F., Selva, J., Frondini, F., Caliro, S., Rosiello, A., Beddini, G., and Ventura, G., 2020, Correlation between tectonic CO2 Earth degassing and seismicity is revealed by a 10-year record in the Apennines, Italy: Science Advances, v. 6, no. 35, https://doi.org/10.1126/sciadv.abc2938.

Cinti, F.R., Pantosti, D., Lombardi, A.M., and Civico, R., 2021, Modeling of earthquake chronology from paleoseismic data: Insights for regional earthquake recurrence and earthquake storms in the Central Apennines: Tectonophysics, v. 816, https://doi.org/10.1016/j.tecto.2021.229016.

Cipriani, A., 2016, Geology of the Mt. Cosce sector (Narni Ridge, Central Apennines, Italy): Journal of Maps, v. 12, p. 328–340, https://doi.org/10.1080/17445647.2016.1211896.

Cipriani, A., 2019, Geological map of the central part of Narni-Amelia Ridge (Central Apennines, Italy): Geological Field Trips and Maps. v. 11, p. 1–26, https://doi.org/10.3301/GFT.2019.04.

Cipriani, A., and Bottini, C., 2019a, Early Cretaceous tectonic rejuvenation of an Early Jurassic margin in the Central Apennines: The "Mt. Cosce Breccia": Sedimentary Geology, v. 387, p. 57–74, https://doi.org/10.1016/j.sedgeo.2019.03.002.

Cipriani, A., and Bottini, C., 2019b, Unconformities, neptunian dykes and mass-transport deposits as an evidence for Early Cretaceous syn-sedimentary tectonics: New insights from the Central Apennines: Italian Journal of Geosciences, v. 138, p. 333–354, https://doi.org/10.3301/IJG.2019.09.

Cipriani, A., Fabbi, S., Lathuilière, B., and Santantonio, M., 2019, A reef coral in the condensed Maiolica facies on the Mt Nerone pelagic carbonate platform (Marche Apennines): The enigma of ancient pelagic deposits: Sedimentary Geology, v. 385, p. 45–60, https://doi.org/10.1016/j.sedgeo.2019.03.007.

Cipriani, A., Caratelli, M., and Santantonio, M., 2020, Geological mapping reveals the role of Early Jurassic rift architecture in the dispersal of calciturbidites: New insights from the Central and Northern Apennines: Basin Research, v. 32, p. 1485–1509, https://doi.org/10.1111/bre.12438.

Cita, M.B., Abbate, E., Ballini, M., Conti, A., Falorni, P., Germani, D., and Petti, F.M., 2007a, Carta Geologica d'Italia 1:50.000. Catalogo delle formazioni—Unità tradizionali (1): Quaderni del Servizio Geologico d'Italia, serie III, v. 7, no. 6, 318 p.

Cita, M.B., Abbate, E., Ballini, M., Conti, A., Falorni, P., Germani, D., and Petti, F.M., 2007b, Carta Geologica d'Italia 1:50.000. Catalogo delle formazioni—Unità tradizionali (2): Quaderni del Servizio Geologico d'Italia, serie III. v. 7, no. 7, 381 p.

Clauer, N., 2013, The K-Ar and $^{40}Ar/^{39}Ar$ methods revisited for dating fine-grained K-bearing clay minerals: Chemical Geology, v. 354, p. 163–185, https://doi.org/10.1016/j.chemgeo.2013.05.030.

Coli, M., and Sani, F., 1990, Vein distribution in a thrust zone: A case history from the Northern Apennines, Italy, *in* Knipe, R.J., and Rutter, E.H., eds., Deformation Mechanisms, Rheology and Tectonics: Geological Society, London, Special Publication 54, p. 475–482, https://doi.org/10.1144/GSL.SP.1990.054.01.43.

Collettini, C., Niemeijer, A., Viti, C., Smith, S.A.F., and Marone, C., 2011, Fault structure, frictional properties and mixed-mode fault slip behavior: Earth and Planetary Science Letters, v. 311, p. 316–327, https://doi.org/10.1016/j.epsl.2011.09.020.

Convertito, V., De Matteis, R., Improta, L., and Pino, N.A., 2020, Fluid-triggered aftershocks in an anisotropic hydraulic conductivity geological complex: The case of the 2016 Amatrice Sequence, Italy: Frontiers of Earth Science, v. 8, https://doi.org/10.3389/feart.2020.541323.

Cooper, J.C., and Burbi, L., 1986, The geology of the central Sibillini Mountains: Memorie della Societa Geologica Italiana, v. 35, p. 323–347.

Corrado, S., Aldega, L., and Zattin, M., 2010, Sedimentary vs. tectonic burial and exhumation along the Apennines (Italy): Journal of the Virtual Explorer, v. 36, https://doi.org/10.3809/jvirtex.2010.00232.

Cosentino, D., Cipollari, P., Marsili, P., and Scrocca, D., 2010, Geology of the central Apennines: A regional review: Journal of the Virtual Explorer, v. 36, https://doi.org/10.3809/jvirtex.2010.00223.

Curzi, M., Aldega, L., Bernasconi, S.M., Berra, F., Billi, A., Boschi, C., Franchini, S., Van der Lelij, R., Viola, G., and Carminati, E., 2020a, Architecture and evolution of an extensionally-inverted thrust (Mt. Tancia Thrust, Central Apennines): Geological, structural, geochemical, and K-Ar geochronological constraints: Journal of Structural Geology, v. 136, https://doi.org/10.1016/j.jsg.2020.104059.

Curzi, M., Billi, A., Carminati, E., Rossetti, F., Albert, R., Aldega, L., Cardello, G.L., Conti, A., Gerdes, A., Smeraglia, L., Van der Lelij, R., Vignaroli, G., and Viola, G., 2020b, Disproving the presence of Paleozoic-Triassic metamorphic rocks on the island of Zannone (central Italy): Implications for the early stages of the Tyrrhenian-Apennines tectonic evolution: Tectonics, v. 39, https://doi.org/10.1029/2020TC006296.

Curzi, M., Bernasconi, S.M., Billi, A., Boschi, C., Aldega, L., Franchini, S., Albert, R., Gerdes, A., Barberio, M.D., Looser, N., and Carminati, E., 2021, U-Pb age of the 2016 Amatrice earthquake causative fault (Mt. Gorzano, Italy) and paleo-fluid circulation during seismic cycles inferred from inter- and co-seismic calcite: Tectonophysics, v. 819, https://doi.org/10.1016/j.tecto.2021.229076.

Deiana, G., and Pieruccini, U., 1971, Primi dati sul Giurassico dei Monti Sibillini: Studi Geologici Camerti, v. 1, p. 91–95.

De Luca, G., di Carlo, G., and Tallini, M., 2018, A record of changes in the Gran Sasso groundwater before, during and after the 2016 Amatrice earthquake, central Italy: Scientific Reports, v. 8, p. 1–16, https://doi.org/10.1038/s41598-018-34444-1.

Deng, H., Bielicki, J.M., Oppenheimer, M., Fitts, J.P., and Peters, C.A., 2017, Leakage risks of geologic CO_2 storage and the impacts on the global energy system and climate change mitigation: Climatic Change, v. 144, p. 151–163, https://doi.org/10.1007/s10584-017-2035-8.

Di Domenica, A., 2012, Geological and structural approach along oblique thrust ramps: The Central-Northern Apennines: Rendiconti Online Societa Geologica Italiana, v. 22, p. 73–75.

Faccenna, C., Becker, T.W., Lucente, F.P., Jolivet, L., and Rossetti, F., 2001, History of subduction and back-arc extension in the Central Mediterranean: Geophysical Journal International, v. 145, p. 809–820, https://doi.org/10.1046/j.0956-540x.2001.01435.x.

Fagereng, Å., and Sibson, R.H., 2010, Mélange rheology and seismic style: Geology, v. 38, p. 751–754, https://doi.org/10.1130/G30868.1.

Farrell, N.J.C., Healy, D., and Taylor, C.W., 2014, Anisotropy of permeability in faulted porous sandstones: Journal of Structural Geology, v. 63, p. 50–67, https://doi.org/10.1016/j.jsg.2014.02.008.

Faulkner, D.R., and Rutter, E.H., 2001, Can the maintenance of overpressured fluids in large strike-slip

fault zones explain their apparent weakness?: Geology, v. 29, no. 6, p. 503–506, https://doi.org/10.1130/0091-7613(2001)029<0503:CTMOOF>2.0.CO;2.

Faulkner, D.R., Lewis, A.C., and Rutter, E.H., 2003, On the internal structure and mechanics of large strike-slip fault zones: Field observations of the Carboneras fault in southeastern Spain: Tectonophysics, v. 367, p. 235–251, https://doi.org/10.1016/S0040-1951(03)00134-3.

Faulkner, D.R., Jackson, C.A.L., Lunn, R.J., Schlische, R.W., Shipton, Z.K., Wibberley, C.A.J., and Withjack, M.O., 2010, A review of recent developments concerning the structure, mechanics and fluid flow properties of fault zones: Journal of Structural Geology, v. 32, p. 1557–1575, https://doi.org/10.1016/j.jsg.2010.06.009.

Fellin, M.G., Jose, M.S., Faccenna, C., Willett, S.D., Cosentino, D., Lanari, R., Gourbet, L., and Maden, C., 2022, Transition from slab roll-back to slab break-off in the central Apennines, Italy: Constraints from the stratigraphic and thermochronologic record: Geological Society of America Bulletin, v. 134, p. 1916–1930, https://doi.org/10.1130/B36123.1.

Fossen, H., Schultz, R.A., and Torabi, A., 2011, Conditions and implications for compaction band formation in the Navajo Sandstone, Utah: Journal of Structural Geology, v. 33, p. 1477–1490, https://doi.org/10.1016/j.jsg.2011.08.001.

Gabrielli, S., Akinci, A., Ventura, G., Napolitano, F., del Pezzo, E., and De Siena, L., 2022, Fast-changes in seismic attenuation of the upper crust due to fracturing and fluid migration: The 2016–2017 Central Italy seismic sequence: Frontiers in Earth Sciences (Lausanne), v. 10, https://doi.org/10.3389/feart.2022.909698.

Galadini, F., and Galli, P., 2003, Paleoseismology of silent faults in the Central Apennines (Italy). The Mt. Vettore and Laga Mts. faults: Annals of Geophysics, v. 46.

Galli, P., Castenetto, S., and Peronace, E., 2017, The macroseismic intensity distribution of the 30 October 2016 earthquake in Central Italy (Mw 6.6): Seismotectonic implications: Tectonics, v. 36, p. 2179–2191, https://doi.org/10.1002/2017TC004583.

Galluzzo, F., and Santantonio, M., 2002, The Sabina Plateau: A new element in the Mesozoic palaeogeography of Central Apennines: Bollettino della Società Geologica Italiana, v. 1, p. 561–588.

Ghisetti, F., Kirschner, D.L., Vezzani, L., and Agosta, F., 2001, Stable isotope evidence for contrasting paleofluid circulation in thrust faults and normal faults of the central Apennines, Italy: Journal of Geophysical Research: Solid Earth, v. 106, p. 8811–8825, https://doi.org/10.1029/2000JB900377.

Giorgetti, C., Collettini, C., Scuderi, M.M., Barchi, M.R., and Tesei, T., 2016, Fault geometry and mechanics of marly carbonate multilayers: An integrated field and laboratory study from the Northern Apennines, Italy: Journal of Structural Geology, v. 93, p. 1–16, https://doi.org/10.1016/j.jsg.2016.10.001.

Gratier, J.P., Dysthe, D.K., and Renard, F., 2013, Chapter 2—the role of pressure solution creep in the ductility of the Earth's upper crust, *in* Dmowska, R., ed., Advances in Geophysics: Amsterdam, Netherlands, Elsevier B.V., v. 54, p. 47–179, https://doi.org/10.1016/B978-0-12-380940-7.00002-0.

Hadizadeh, J., 1994, Interaction of cataclasis and pressure solution in a low-temperature carbonate shear zone: Pure and Applied Geophysics, v. 143, p. 255–280, https://doi.org/10.1007/BF00874331.

Harding, T.P., and Lowell, J.D., 1979, Structural Styles, Their plate-tectonic habitats, and hydrocarbon traps in petroleum provinces: The American Association of Petroleum Geologists Bulletin, v. 63, p. 1016–1058.

Heinemann, N., Booth, M.G., Haszeldine, R.S., Wilkinson, M., Scafidi, J., and Edlmann, K., 2018, Hydrogen storage in porous geological formations: Onshore play opportunities in the midland valley (Scotland, UK): International Journal of Hydrogen Energy, v. 43, p. 20,861–20,874, https://doi.org/10.1016/j.ijhydene.2018.09.149.

Ikari, M.J., Saffer, D.M., and Marone, C., 2009, Frictional and hydrologic properties of clay-rich fault gouge: Journal of Geophysical Research: Solid Earth, v. 114, https://doi.org/10.1029/2008JB006089.

Improta, L., Latorre, D., Margheriti, L., Nardi, A., Marchetti, A., Lombardi, A.M., Castello, B., Villani, F., Ciaccio, M.G., Mele, F.M., and Moretti, M., and The Bollettini Sismico Italiano Working Group, 2019, Multi-segment rupture of the 2016 Amatrice-Visso-Norcia seismic sequence (central Italy) constrained by the first high-quality catalog of Early Aftershocks: Scientific Reports, v. 9, p. 1–13, https://doi.org/10.1038/s41598-019-43393-2.

Ingram, G.M., Chisholm, T.J., Grant, C.J., Hedlund, C.A., Stuart-Smith, P., and Teasdale, J., 2004, Deepwater North West Borneo: Hydrocarbon accumulation in an active fold and thrust belt: Marine and Petroleum Geology, v. 21, p. 879–887, https://doi.org/10.1016/j.marpetgeo.2003.12.007.

Jansen, G., Ruhl, C.J., and Miller, S.A., 2019, Fluid pressure-triggered foreshock sequence of the 2008 Mogul earthquake sequence: Insights from stress inversion and numerical modeling: Journal of Geophysical Research: Solid Earth, v. 124, p. 3744–3765, https://doi.org/10.1029/2018JB015897.

Kawano, S., Katayama, I., and Okazaki, K., 2011, Permeability anisotropy of serpentinite and fluid pathways in a subduction zone: Geology, v. 39, p. 939–942, https://doi.org/10.1130/G32173.1.

Kennedy, L.A., and Logan, J.M., 1997, The role of veining and dissolution in the evolution of fine-grained mylonites: The McConnell thrust, Alberta: Journal of Structural Geology, v. 19, no. 6, p. 785–797, https://doi.org/10.1016/S0191-8141(97)00005-9.

King Hubbert, M., and Rubey, W.W., 1959, Role of fluid pressure in mechanics of overthrust faulting: I. Mechanics of fluid-filled porous solids and its application to overthrust faulting: Geological Society of America Bulletin, v. 70, p. 115–166, https://doi.org/10.1130/0016-7606(1959)70[115:ROFPIM]2.0.CO;2.

Labeur, A., Beaudoin, N.E., Lacombe, O., Emmanuel, L., Petracchini, L., Daëron, M., Klimowicz, S., and Callot, J.-P., 2021, Burial-deformation history of folded rocks unraveled by fracture analysis, stylolite paleopiezometry and vein cement geochemistry: A case study in the Cingoli Anticline (Umbria-Marche, Northern Apennines): Geosciences, v. 11, p. 135, https://doi.org/10.3390/geosciences11030135.

Lacombe, O., Lavè, J., Roure, F.M., and Verges, J., eds., 2007, Thrust belts and foreland basins: From fold kinematics to hydrocarbon systems: Frontiers in Earth Sciences Series, Berlin-Heidelberg, Germany, Springer Science & Business Media, 308 p., https://doi.org/10.1007/978-3-540-69426-7.

Lacombe, O., Beaudoin, N.E., Hoareau, G., Labeur, A., Pecheyran, C., and Callot, J.P., 2021, Dating folding beyond folding, from layer-parallel shortening to fold tightening, using mesostructures: Lessons from the Apennines, Pyrenees, and Rocky Mountains: Solid Earth, v. 12, p. 2145–2157, https://doi.org/10.5194/se-12-2145-2021.

Lacroix, B., Baumgartner, L.P., Bouvier, A.S., Kempton, P.D., and Vennemann, T., 2018, Multi fluid-flow record during episodic mode I opening: A microstructural and SIMS study (Cotiella Thrust Fault, Pyrenees): Earth and Planetary Science Letters, v. 503, p. 37–46, https://doi.org/10.1016/j.epsl.2018.09.016.

Lavecchia, G., Castaldo, R., De Nardis, R., De Novellis, V., Ferrarini, F., Pepe, S., Brozzetti, F., Solaro, G., Cirillo, D., Bonano, M., Boncio, P., Casu, F., De Luca, C., Lanari, R., Manunta, M., Manzo, M., Pepe, A., Zinno, I., and Tizzani, P., 2016, Ground deformation and source geometry of the 24 August 2016 Amatrice earthquake (Central Italy) investigated through analytical and numerical modeling of DInSAR measurements and structural-geological data: Geophysical Research Letters, v. 43, p. 12,389–12,398, https://doi.org/10.1002/2016GL071723.

Lena, G., Barchi, M.R., Alvarez, W., Felici, F., and Minelli, G., 2015, Mesostructural analysis of S-C fabrics in a shallow shear zone of the Umbria-Marche Apennines (Central Italy), *in* Faulkner, D.R., Mariani, E., and Mecklenburgh, J., eds., Rock Deformation from Field, Experiments and Theory: A Volume in Honour of Ernie Rutter: Geological Society, London, Special Publication 409, p. 149–166, https://doi.org/10.1144/SP409.10.

Leoni, L., Vannucchi, P., Principi, G., and Catani, F., 2007, Deformation pattern in the underthrust carbonate-rich sequence of the Sibillini Thrust (central Italy): Insights for shear zone evolution in modern subduction complexes: Geodinamica Acta, v. 20, p. 53–69, https://doi.org/10.3166/ga.20.53-69.

Malagnini, L., Parsons, T., Munafò, I., Mancini, S., Segou, M., and Geist, E.L., 2022, Crustal permeability changes inferred from seismic attenuation: Impacts on multi-mainshock sequences: Frontiers of Earth Science, v. 10, https://doi.org/10.3389/feart.2022.963689.

Malinverno, A., and Ryan, W.B.F., 1986, Extension in the Tyrrhenian Sea and shortening in the Apennines as result of arc migration driven by sinking of the lithosphere: Tectonics, v. 5, p. 227–245, https://doi.org/10.1029/TC005i002p00227.

Mancinelli, P., Porreca, M., Pauselli, C., Minelli, G., Barchi, M.R., and Speranza, F., 2019, Gravity and magnetic modeling of Central Italy: Insights into the depth extent of the seismogenic layer: Geochemistry, Geophysics, Geosystems, v. 20, p. 2157–2172, https://doi.org/10.1029/2018GC008002.

Martinelli, G., Facca, G., Genzano, N., Gherardi, F., Lisi, M., Pierotti, L., and Tramutoli, V., 2020, Earthquake-related signals in Central Italy detected by hydrogeochemical and satellite techniques: Frontiers of Earth Science, v. 8, https://doi.org/10.3389/feart.2020.584716.

Mastrorillo, L., and Petitta, M., 2014, Hydrogeological conceptual model of the upper Chienti River Basin aquifers (Umbria-Marche Apennines): Italian Journal of Geosciences, v. 133, p. 396–408, https://doi.org/10.3301/IJG.2014.12.

Mastrorillo, L., Saroli, M., Viaroli, S., Banzato, F., Valigi, D., and Petitta, M., 2020, Sustained post-seismic effects on groundwater flow in fractured carbonate aquifers in Central Italy: Hydrological Processes, v. 34, p. 1167–1181, https://doi.org/10.1002/hyp.13662.

Mazzoli, S., Pierantoni, P.P., Borraccini, F., Paltrinieri, W., and Deiana, G., 2005, Geometry, segmentation pattern and displacement variations along a major Apennine thrust zone, central Italy: Journal of Structural Geology, v. 27, p. 1940–1953, https://doi.org/10.1016/j.jsg.2005.06.002.

Michele, M., Chiaraluce, L., di Stefano, R., and Waldhauser, F., 2020, Fine-scale structure of the 2016–2017 central Italy seismic sequence from data recorded at the Italian national network: Journal of Geophysical Research: Solid Earth, v. 125, p. 1–26, https://doi.org/10.1029/2019JB018440.

Miller, S.A., Collettini, C., Chiaraluce, L., Cocco, M., Barchi, M., and Kaus, B.J.P., 2004, Aftershocks driven by a high-pressure CO_2 source at depth: Nature, v. 427, p. 724–727, https://doi.org/10.1038/nature02251.

Mitra, S., 1986, Duplex structures and imbricate thrust systems: Geometry, structural position, and hydrocarbon potential: American Association of Petroleum Geologists Bulletin, v. 70, p. 1087–1112, http://pubs.geoscienceworld.org/aapgbull/article-pdf/70/9/1087/4476960/aapg_1986_0070_0009_1087.pdf.

Mitra, S., 1990, Fault-propagation folds: Geometry, kinematic evolution, and hydrocarbon traps: The American Association of Petroleum Geologists Bulletin, v. 74, p. 921–945.

Mittempergher, S., Di Toro, G., Gratier, J.P., Hadizadeh, J., Smith, S.A.F., and Spiess, R., 2011, Evidence of transient increases of fluid pressure in SAFOD phase III cores: Geophysical Research Letters, v. 38, https://doi.org/10.1029/2010GL046129.

Muhammed, N.S., Haq, B., al Shehri, D., Al-Ahmed, A., Rahman, M.M., and Zaman, E., 2022, A review on underground hydrogen storage: Insight into geological sites, influencing factors and future outlook: Energy Reports, v. 8, p. 461–499, https://doi.org/10.1016/j.egyr.2021.12.002.

Muñoz-López, D., Cruset, D., Cantarero, I., Benedicto, A., John, C.M., and Travé, A., 2020, Fluid dynamics in a thrust fault inferred from petrology and geochemistry of calcite veins: An example from the Southern Pyrenees: Geofluids, v. 2020, https://doi.org/10.1155/2020/8815729.

Nanni, T., and Vivalda, P., 2005, The aquifers of the Umbria-Marche Adriatic region: Relationships between structural setting and groundwater chemistry: Bollettino della Società Geologica Italiana, v. 124, p. 523–524.

Pace, P., and Calamita, F., 2014, Push-up inversion structures v. fault-bend reactivation anticlines along oblique thrust

ramps: Examples from the Apennines fold-and-thrust belt (Italy): Journal of the Geological Society, v. 171, p. 227–238, https://doi.org/10.1144/jgs2013-053.

Pace, P., Calamita, F., and Tavarnelli, E., 2015, Brittle-ductile shear zones along inversion-related frontal and oblique thrust ramps, *in* Mukherjee, S., and Mulchrone, K.F., eds., Ductile Shear Zones: Chichester, UK, John Wiley & Sons, Ltd., p. 111–127, https://doi.org/10.1002/9781118844953.ch8.

Pace, P., Calamita, F., and Tavarnelli, E., 2022a, Along-strike variation of fault-related inversion folds within curved thrust systems: The case of the Central-Northern Apennines of Italy: Marine and Petroleum Geology, v. 142, https://doi.org/10.1016/j.marpetgeo.2022.105731.

Pace, P., Calamita, F., and Tavarnelli, E., 2022b, Shear zone fabrics and their significance in curved, inverted basin-derived thrust systems: Journal of Structural Geology, v. 161, https://doi.org/10.1016/j.jsg.2022.104663.

Pană, D.I., and Van der Pluijm, B.A., 2015, Orogenic pulses in the Alberta Rocky Mountains: Radiometric dating of major faults and comparison with the regional tectono-stratigraphic record: Geological Society of America Bulletin, v. 127, p. 480–502, https://doi.org/10.1130/B31069.1.

Patacca, E., Sartori, R., and Scandone, P., 1990, Tyrrhenian basin and Apenninic arcs: Kinematic relations since Late Tortonian times: Memorie della Societa Geologica Italiana, v. 45, p. 425–451.

Petitta, M., Mastrorillo, L., Preziosi, E., Banzato, F., Barberio, M.D., Billi, A., Cambi, C., De Luca, G., Di Carlo, G., Curzio, D., Di Salvo, C., Nanni, T., Palpacelli, S., Rusi, S., Saroli, M., Tallini, M., Tazioli, A., Valigi, D., Vivalda, P., and Doglioni, C., 2018, Water-table and discharge changes associated with the 2016–2017 seismic sequence in central Italy: Hydrogeological data and a conceptual model for fractured carbonate aquifers: Hydrogeology Journal, v. 26, p. 1009–1026, https://doi.org/10.1007/s10040-017-1717-7.

Pevear, D.R., 1999, Illite and hydrocarbon exploration: Proceedings of the National Academy of Sciences of the United States of America, v. 96, p. 3440–3446, https://doi.org/10.1073/pnas.96.7.3440.

Pierantoni, P., Deiana, G., and Galdenzi, S., 2013, Stratigraphic and structural features of the Sibillini Mountains (Umbria-Marche Apennines, Italy): Italian Journal of Geosciences, v. 132, p. 497–520, https://doi.org/10.3301/IJG.2013.08.

Pizzi, A., and Galadini, F., 2009, Pre-existing cross-structures and active fault segmentation in the northern-central Apennines (Italy): Tectonophysics, v. 476, p. 304–319, https://doi.org/10.1016/j.tecto.2009.03.018.

Pizzi, A., di Domenica, A., Gallovič, F., Luzi, L., and Puglia, R., 2017, Fault segmentation as constraint to the occurrence of the main shocks of the 2016 Central Italy Seismic Sequence: Tectonics, v. 36, p. 2370–2387, https://doi.org/10.1002/2017TC004652.

Porreca, M., Minelli, G., Ercoli, M., Brobia, A., Mancinelli, P., Cruciani, F., Giorgetti, C., Carboni, F., Mirabella, F., Cavinato, G., Cannata, A., Pauselli, C., and Barchi, M.R., 2018, Seismic reflection profiles and subsurface geology of the area interested by the 2016–2017 earthquake sequence (Central Italy): Tectonics, v. 37, p. 1116–1137, https://doi.org/10.1002/2017TC004915.

Porreca, M., Fabbrizzi, A., Azzaro, S., Pucci, S., del Rio, L., Pierantoni, P.P., Giorgetti, C., Roberts, G., and Barchi, M.R., 2020, 3D geological reconstruction of the M. Vettore seismogenic fault system (Central Apennines, Italy): Cross-cutting relationship with the M. Sibillini thrust: Journal of Structural Geology, v. 131, https://doi.org/10.1016/j.jsg.2019.103938.

Rutter, E.H., 1976, A discussion on natural strain and geological structure—the kinetics of rock deformation by pressure solution: Philosophical Transactions of the Royal Society of London, Series A, Mathematical and Physical Sciences, v. 283, p. 203–219, https://doi.org/10.1098/rsta.1976.0079.

Santantonio, M., 1993, Facies associations and evolution of pelagic carbonate platform/basin systems: Examples from the Italian Jurassic: Sedimentology, v. 40, p. 1039–1067, https://doi.org/10.1111/j.1365-3091.1993.tb01379.x.

Santantonio, M., 1994, Pelagic carbonate platforms in the geologic record: Their classification, and sedimentary and paleotectonic evolution: The American Association of Petroleum Geologists Bulletin, v. 78, p. 122–141.

Santantonio, M., and Carminati, E., 2011, Jurassic rifting evolution of the Apennines and Southern Alps (Italy): Parallels and differences: Geological Society of America Bulletin, v. 123, p. 468–484, https://doi.org/10.1130/B30104.1.

Santantonio, M., Fabbi, S., and Aldega, L., 2016, Mesozoic architecture of a tract of the European–Iberian continental margin: Insights from preserved submarine palaeotopography in the Longobucco Basin (Calabria, Southern Italy): Sedimentary Geology, v. 331, p. 94–113, https://doi.org/10.1016/j.sedgeo.2015.10.010.

Santantonio, M., Cipriani, A., Fabbi, S., and Meister, C., 2022, Constraining the slip rate of Jurassic rift faults through the drowning history of a carbonate platform: Terra Nova, v. 34, p. 137–145, https://doi.org/10.1111/ter.12575.

Satolli, S., Robustelli Test, C., Staneczek, D., Zanella, E., Calamita, F., and Tema, E., 2020, Magnetic fabric in carbonatic rocks from thrust shear zones: A study from the Northern Apennines (Italy): Tectonophysics, v. 791, https://doi.org/10.1016/j.tecto.2020.228573.

Schimmel, M., Liu, W., and Worrell, E., 2019, Facilitating sustainable geo-resources exploitation: A review of environmental and geological risks of fluid injection into hydrocarbon reservoirs: Earth-Science Reviews, v. 194, p. 455–471, https://doi.org/10.1016/j.earscirev.2019.03.006.

Scisciani, V., Agostini, S., Calamita, F., Pace, P., Cilli, A., Giori, I., and Paltrinieri, W., 2014, Positive inversion tectonics in foreland fold-and-thrust belts: A reappraisal of the Umbria-Marche Northern Apennines (Central Italy) by integrating geological and geophysical data: Tectonophysics, v. 637, p. 218–237, https://doi.org/10.1016/j.tecto.2014.10.010.

Scisciani, V., Patruno, S., Tavarnelli, E., Calamita, F., Pace, P., and Iacopini, D., 2019, Multi-phase reactivations and inversions of Paleozoic–Mesozoic extensional basins during the Wilson cycle: Case studies from the North Sea (UK) and the Northern Apennines (Italy), *in* Wilson, R.W., Houseman, G.A., McCaffrey, K.J.W., Doré, A.G., Buiter, S.J.H., eds., Fifty Years of the Wilson Cycle Concept in Plate Tectonics: Geological Society, London, Special Publication 470, p. 205–243, https://doi.org/10.1144/SP470-2017-232.

Scognamiglio, L., Tinti, E., and Quintiliani, M., 2016, The first month of the 2016 central Italy seismic sequence: Fast determination of time domain moment tensors and finite fault model analysis of the ML 5.4 aftershock: Annals of Geophysics, v. 59, https://doi.org/10.4401/ag-7246.

Scognamiglio, L., Tinti, E., Casarotti, E., Pucci, S., Villani, F., Cocco, M., Magnoni, F., Michelini, A., and Dreger, D., 2018, Complex fault geometry and rupture dynamics of the MW 6.5, 30 October 2016, Central Italy Earthquake: Journal of Geophysical Research: Solid Earth, v. 123, p. 2943–2964, https://doi.org/10.1002/2018JB015603.

Scuderi, M.M., and Collettini, C., 2018, Fluid injection and the mechanics of frictional stability of shale-bearing faults: Journal of Geophysical Research: Solid Earth, v. 123, p. 8364–8384, https://doi.org/10.1029/2018JB016084.

Sibson, R.H., 1981, Fluid flow accompanying faulting: Field evidence and models: Earthquake prediction: An international review, v. 4, p. 593–603, https://www.researchgate.net/publication/279590829.

Sibson, R.H., 1990, Conditions for fault-valve behaviour, *in* Knipe, R.J., and Rutter, E.H., eds., Deformation Mechanisms, Rheology and Tectonics: Geological Society, London, Special Publication 54, p. 15–28, https://doi.org/10.1144/GSL.SP.1990.054.01.02.

Sibson, R.H., 1992, Implications of fault-valve behavior for rupture nucleation and recurrence: Tectonophysics, v. 211, no. 1–4, p. 283–293, https://doi.org/10.1016/0040-1951(92)90065-E.

Sibson, R.H., 2000, Fluid involvement in normal faulting: Journal of Geodynamics, v. 29, p. 469–499, https://doi.org/10.1016/S0264-3707(99)00042-3.

Sibson, R.H., 2007, An episode of fault-valve behaviour during compressional inversion?: The 2004 M_J6.8 Mid-Niigata Prefecture, Japan, earthquake sequence: Earth and Planetary Science Letters, v. 257, p. 188–199, https://doi.org/10.1016/j.epsl.2007.02.031.

Sibson, R.H., and Rowland, J.V., 2003, Stress, fluid pressure and structural permeability in seismogenic crust, North Island, New Zealand: Geophysical Journal International, v. 154, p. 584–594, https://doi.org/10.1046/j.1365-246X.2003.01965.x.

Smeraglia, L., Aldega, L., Bernasconi, S.M., Billi, A., Boschi, C., Caracausi, A., Carminati, E., Franchini, S., Rizzo, A.L., Rossetti, F., and Vignaroli, G., 2020, The role of trapped fluids during the development and deformation of a carbonate/shale intra-wedge tectonic mélange (Mt. Massico, Southern Apennines, Italy): Journal of Structural Geology, v. 138, https://doi.org/10.1016/j.jsg.2020.104086.

Spiers, C.J., Hangx, S.J.T., and Niemeijer, A.R., 2017, New approaches in experimental research on rock and fault behaviour in the Groningen gas field: Geologie en Mijnbouw: Netherlands Journal of Geosciences, v. 96, p. s55–s69, https://doi.org/10.1017/njg.2017.32.

Stendardi, F., Capotorti, F., Fabbi, S., Ricci, V., Silvestri, S., and Bigi, S., 2020, Geological map of the Mt. Vettoretto-Capodacqua area (Central Apennines, Italy) and cross-cutting relationships between Sibillini Mts. Thrust and Mt. Vettore normal faults system: Geological Field Trips and Maps, v. 12, p. 1–22, https://doi.org/10.3301/GFT.2020.04.

Suppe, J., 2014, Fluid overpressures and strength of the sedimentary upper crust: Journal of Structural Geology, v. 69, p. 481–492, https://doi.org/10.1016/j.jsg.2014.07.009.

Tartaglia, G., Viola, G., van der Lelij, R., Scheiber, T., Ceccato, A., and Schönenberger, J., 2020, "Brittle structural facies" analysis: A diagnostic method to unravel and date multiple slip events of long-lived faults: Earth and Planetary Science Letters, v. 545, https://doi.org/10.1016/j.epsl.2020.116420.

Tavani, S., Storti, F., Baus, J., and Muoz, J.A., 2012, Late thrusting extensional collapse at the mountain front of the northern Apennines (Italy): Tectonics, v. 31, https://doi.org/10.1029/2011TC003059.

Tavani, S., Storti, F., Lacombe, O., Corradetti, A., Muñoz, J.A., and Mazzoli, S., 2015, A review of deformation pattern templates in foreland basin systems and fold-and-thrust belts: Implications for the state of stress in the frontal regions of thrust wedges: Earth-Science Reviews, v. 141, p. 82–104, https://doi.org/10.1016/j.earscirev.2014.11.013.

Tavarnelli, E., 1993, Evidence for fault propagation folding in the Umbria-Marche-Sabina Apennines (Central Italy): Annales Tectonicae, v. 7, p. 87–99.

Tavarnelli, E., Butler, R.W.H., Decandia, F.A., Calamita, F., Grasso, M., Alvarez, W., and Renda, P., 2004, Implications of fault reactivation and structural inheritance in the Cenozoic tectonic evolution of Italy: The Geological Society of Italy Special Publication 1, p. 209–222.

Tavarnelli, E., Scisciani, V., Patruno, S., Calamita, F., Pace, P., and Iacopini, D., 2019, The role of structural inheritance in the evolution of fold-and-thrust belts: Insights from the Umbria-Marche Apennines, Italy, *in* Koeberl, C., and Bice, D.M., eds., 250 Million Years of Earth History in Central Italy: Celebrating 25 Years of the Geological Observatory of Coldigioco: Geological Society of America Special Paper 542, p. 191–211, https://doi.org/10.1130/2019.2542(10).

Tesei, T., Collettini, C., Viti, C., and Barchi, M.R., 2013, Fault architecture and deformation mechanisms in exhumed analogues of seismogenic carbonate-bearing thrusts: Journal of Structural Geology, v. 55, p. 167–181, https://doi.org/10.1016/j.jsg.2013.07.007.

Tesei, T., Collettini, C., Barchi, M.R., Carpenter, B.M., and di Stefano, G., 2014, Heterogeneous strength and fault zone complexity of carbonate-bearing thrusts with possible implications for seismicity: Earth and Planetary Science Letters, v. 408, p. 307–318, https://doi.org/10.1016/j.epsl.2014.10.021.

Torgersen, E., and Viola, G., 2014, Structural and temporal evolution of a reactivated brittle-ductile fault—part I: Fault architecture, strain localization mechanisms and deformation history: Earth and Planetary Science Letters, v. 407, p. 205–220, https://doi.org/10.1016/j.epsl.2014.09.019.

Torgersen, E., Viola, G., Zwingmann, H., and Harris, C., 2015, Structural and temporal evolution of a reactivated

brittle-ductile fault—part II: Timing of fault initiation and reactivation by K-Ar dating of synkinematic illite/muscovite: Earth and Planetary Science Letters, v. 410, p. 212–224, https://doi.org/10.1016/j.epsl.2014.09.051.

Trippetta, F., Collettini, C., Vinciguerra, S., and Meredith, P.G., 2010, Laboratory measurements of the physical properties of Triassic Evaporites from Central Italy and correlation with geophysical data: Tectonophysics, v. 492, p. 121–132, https://doi.org/10.1016/j.tecto.2010.06.001.

Turtù, A., Satolli, S., Maniscalco, R., Calamita, F., and Speranza, F., 2013, Understanding progressive-arc- and strike-slip-related rotations in curve-shaped orogenic belts: The case of the Olevano-Antrodoco-Sibillini thrust (Northern Apennines, Italy): Journal of Geophysical Research: Solid Earth, v. 118, p. 459–473, https://doi.org/10.1002/jgrb.50096.

Uysal, I.T., Feng, Y., Zhao, J., Bolhar, R., Işik, V., Baublys, K.A., Yago, A., and Golding, S.D., 2011, Seismic cycles recorded in late Quaternary calcite veins: Geochronological, geochemical and microstructural evidence: Earth and Planetary Science Letters, v. 303, p. 84–96, https://doi.org/10.1016/j.epsl.2010.12.039.

Van der Pluijm, B.A., Hall, C.M., Vrolijk, P.J., Pevear, D.R., and Covey, M.C., 2001, The dating of shallow faults in the earth's crust: Nature, v. 412, p. 172–175, https://doi.org/10.1038/35084053.

Vannucchi, P., 2019, Scaly fabric and slip within fault zones: Geosphere, v. 15, p. 342–356, https://doi.org/10.1130/GES01651.1.

Vannucchi, P., Maltman, A., Bettelli, G., and Clennell, B., 2003, On the nature of scaly fabric and scaly clay: Journal of Structural Geology, v. 25, p. 673–688, https://doi.org/10.1016/S0191-8141(02)00066-4.

Viaroli, S., Mirabella, F., Mastrorillo, L., Angelini, S., and Valigi, D., 2021, Fractured carbonate aquifers of Sibillini Mts. (Central Italy): Journal of Maps, v. 17, p. 140–149, https://doi.org/10.1080/17445647.2021.1894252.

Vignaroli, G., Aldega, L., Balsamo, F., Billi, A., de Benedetti, A.A., de Filippis, L., Giordano, G., and Rossetti, F., 2015, A way to hydrothermal paroxysm, Colli Albani volcano, Italy: Geological Society of America Bulletin, v. 127, p. 672–687, https://doi.org/10.1130/B31139.1.

Vignaroli, G., Viola, G., Diamanti, R., Zuccari, C., Garofalo, P.S., Bonini, S., and Selli, L., 2020, Multistage strain localisation and fluid-assisted cataclasis in carbonate rocks during the seismic cycle: Insights from the Belluno Thrust (eastern Southern Alps, Italy): Journal of Structural Geology, v. 141, https://doi.org/10.1016/j.jsg.2020.104216.

Vignaroli, G., Rossetti, F., Petracchini, L., Argante, V., Bernasconi, S.M., Brilli, M., Giustini, F., Yu, T.L., Shen, C.C., and Soligo, M., 2022, Middle Pleistocene fluid infiltration with 10–15 ka recurrence within the seismic cycle of the active Monte Morrone Fault System (central Apennines, Italy): Tectonophysics, v. 827, https://doi.org/10.1016/j.tecto.2022.229269.

Viola, G., Mancktelow, N.S., and Miller, J.A., 2006, Cyclic frictional-viscous slip oscillations along the base of an advancing nappe complex: Insights into the brittle-ductile nappe emplacement mechanisms from the Naukluft Nappe Complex, central Namibia: Tectonics, v. 25, no. 3, https://doi.org/10.1029/2005TC001939.

Viola, G., Torgersen, E., Mazzarini, F., Musumeci, G., Van der Lelij, R., Schönenberger, J., and Garofalo, P.S., 2018, New Constraints on the evolution of the inner Northern Apennines by K-Ar dating of late Miocene-early Pliocene compression on the Island of Elba, Italy: Tectonics, v. 37, p. 3229–3243, https://doi.org/10.1029/2018TC005182.

Viola, G., Musumeci, G., Mazzarini, F., Tavazzani, L., Curzi, M., Torgersen, E., Van der Lelij, R., and Aldega, L., 2022, Structural characterization and K-Ar illite dating of reactivated, complex and heterogeneous fault zones: Lessons from the Zuccale Fault, Northern Apennines: Solid Earth, v. 13, p. 1327–1351, https://doi.org/10.5194/se-13-1327-2022.

Wenning, Q.C., Madonna, C., Zappone, A., Grab, M., Rinaldi, A.P., Plötze, M., Nussbaum, C., Giardini, D., and Wiemer, S., 2021, Shale fault zone structure and stress dependent anisotropic permeability and seismic velocity properties (Opalinus Clay, Switzerland): Journal of Structural Geology, v. 144, https://doi.org/10.1016/j.jsg.2020.104273.

Wibberley, C.A.J., Yielding, G., and di Toro, G., 2008, Recent advances in the understanding of fault zone internal structure: A review, *in* Wibberley, C.A.J., Kurz, W., Imber, J., Holdsworth, R.E., and Collettini, C., eds., The Internal Structure of Fault Zones: Implications for Mechanical and Fluid-Flow Properties: Geological Society, London, Special Publication 299, p. 5–33, https://doi.org/10.1144/SP299.2.

Williams, R.T., Goodwin, L.B., Sharp, W.D., and Mozley, P.S., 2017, Reading a 400,000-year record of earthquake frequency for an intraplate fault: Proceedings of the National Academy of Sciences of the United States of America, v. 114, p. 4893–4898, https://doi.org/10.1073/pnas.1617945114.

Wu, J., Fan, T., Gomez-Rivas, E., Cao, Q., Travé, A., Gao, Z., Kang, Z., Koehn, D., and Bons, P.D., 2023, Relationship between stylolite morphology and the sealing potential of stylolite-bearing carbonate cap rocks: Geological Society of America Bulletin, v. 135, https://doi.org/10.1130/B36297.1.

York, D., Evensen, N.M., Martínez, M.L., and de Basabe Delgado, J., 2004, Unified equations for the slope, intercept, and standard errors of the best straight line: American Journal of Physics, v. 72, p. 367–375, https://doi.org/10.1119/1.1632486.

Zuccari, C., Viola, G., Curzi, M., Aldega, L., and Vignaroli, G., 2022, What steers the "folding to faulting" transition in carbonate-dominated seismic fold-and-thrust belts?: New insights from the Eastern Southern Alps (Northern Italy): Journal of Structural Geology, v. 157, https://doi.org/10.1016/j.jsg.2022.104560.

Science Editor: Wenjiao Xiao
Associate Editor: Enrico Tavarnelli

Manuscript Received 2 June 2022
Revised Manuscript Received 26 November 2022
Manuscript Accepted 16 December 2022

Printed in the USA